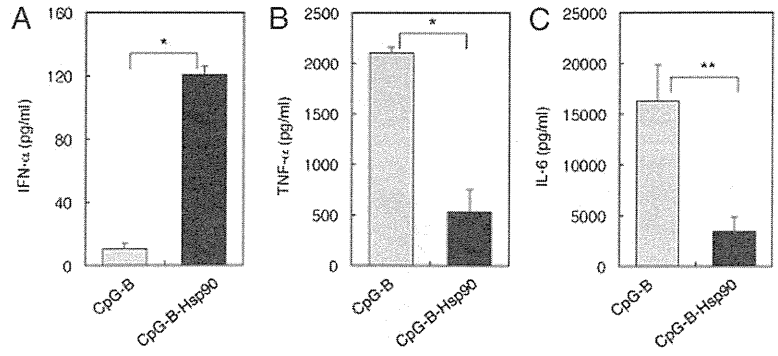

FIGURE 7. Hsp90 converts CpG-B to a trigger of IFN-α production by cDCs. IFN-α (*A*), TNF-α (*B*), and IL-6 (*C*) production poststimulation with 3 μM CpG-B or in complex with Hsp90 by cDCs. Data are presented as means + SEM of triplicate wells. Data are representative of three independent experiments. $*p < 0.005$; $**p < 0.01$, paired Student *t* test.

CD86 and the expression of MHC class II molecules. Recently, it has been demonstrated that the manner of CpG internalization and the retention time of CpG in endosomes differ between CpG-A and CpG-B, and the retention of the CpG/TLR9 complex in endosomes is the primary determinant of TLR signaling (17, 34). CpG-A ODNs are characterized by a poly G tail that forms large multimeric aggregates with a diameter ~50 μm. In contrast, CpG-B ODNs are monomeric and do not form such higher order structures. In addition, multimeric CpG-A ODNs are retained for longer periods of time in the early endosomes, whereas CpG-B ODNs rapidly traffic through early endosomes into late endosomes or lysosomes of pDCs. The prolonged retention of multimeric CpG-A ODNs provides extended activation of the TLR9-MyD88-IRF7 signal-transducing complex, which leads to robust IFN-α production. Therefore, we also examined the ability of Hsp90 to target and retain chaperoned CpG-DNA in static early endosomes of cDCs, resulting in type I IFN production. We found that Hsp90-chaperoned CpG-A was localized and retained within static early endosomes for longer periods in cDCs, thereby eliciting TLR9 signaling for IFN-α production, but not inflammatory cytokines, such as IL-6 and TNF-α. In contrast, CpG-A alone moved into late endosomes and lysosomes within cDCs. Interestingly, not only CpG-A but also CpG-B could stimulate the TLR9 signaling within static early endosomes, resulting in the production of IFN-α. Thus, extracellular Hsp90 had the ability to direct associated molecules into static early endosomes. Moreover, as time passed, the CpG-A–Hsp90 complex formed large aggregates within early endosomes (Fig. 6*B*), again suggesting an important link between the physical size of TLR9 ligands and their stimulatory capacity. Thus, our data indicated that when DCs detected aggregated DNA structures in the early endosomes through TLR9, this was coupled with IRF7 activation and IFN-α production. By contrast, when DCs sensed the linear DNA structures in the late endosomes or lysosomes through TLR9, this was coupled with NF-κB activation, which led to IL-6 and TNF-α production and DC maturation.

Why, however, are DNA–Hsp90 complexes selectively retained in early endosomes but not in late endosomes or lysosomes in DCs? We found that endocytosed CpG-A–Hsp90 complexes were selectively transferred into $Rab5^+$, $EEA\text{-}1^+$-static early endosomes. Very recently, Lakadamyali et al. (31) have shown that early endosomes are comprised of two distinct populations: a dynamic population that is highly mobile on microtubules and matures rapidly toward the late endosome and a static population that matures much more slowly. Cargos destined for degradation, including low-density lipoprotein, epidermal growth factor, and influenza virus, are internalized and targeted to the $Rab5^+$, $EEA1^-$ dynamic population of early endosomes, thereafter trafficking to $Rab7^+$ late endosomes. In contrast, the recycling ligand

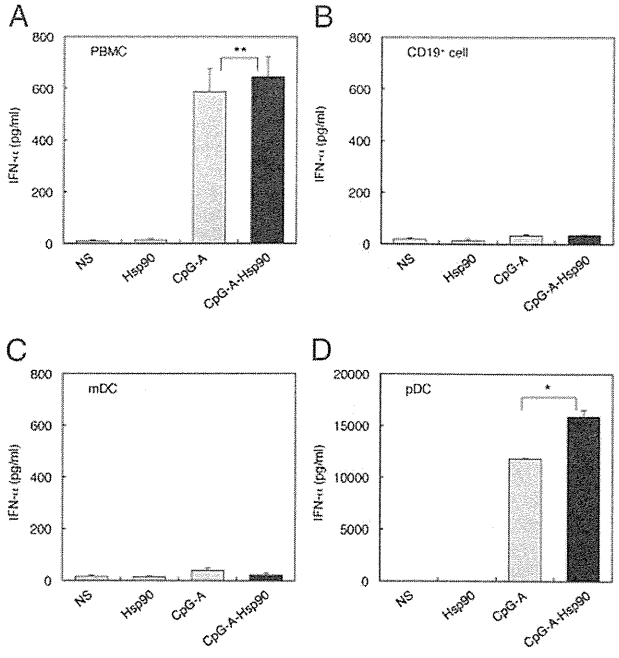

FIGURE 8. CpG-A–Hsp90 complex enhances IFN-α induction by human pDCs. IFN-α production poststimulation with NS, Hsp90, 3 μM CpG-A alone or in complex with Hsp90 by human PBMC (*A*), $CD19^+$ cells (*B*), mDCs (*C*), and pDCs (*D*). Data are presented as means + SEM of triplicate wells. Data are representative of three independent experiments. $*p < 0.005$, $**p < 0.05$, paired Student *t* test. NS, normal saline.

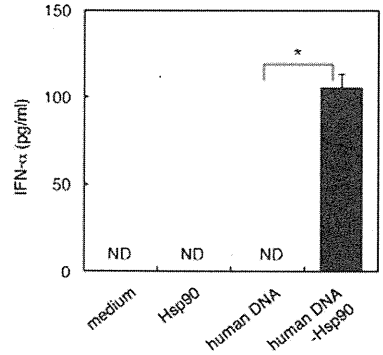

FIGURE 9. Hsp90 converts self-DNA into a potent trigger of IFN-α induction by human pDCs. Human pDCs were stimulated with genomic DNA isolated from healthy volunteers (10 μg/ml) either alone or postcomplexing with Hsp90 (10 μg). Levels of IFN-α were measured after overnight culture using ELISA. Error bars represent the SEM of triplicate wells. Data are representative of four independent experiments. $*p < 0.005$, paired Student *t* test. ND, not detected.

transferrin is delivered to Rab5$^+$, EEA1$^+$-static early endosomes, followed by translocation to Rab11$^+$ recycling endosomes. They also found that cargos trafficked into these static early endosomes were retained for longer periods and not translocated into late endosomes and lysosomes. Therefore, our observation that the CpG-A–Hsp90 complex was retained in the static early endosomes, leading to sustained activation of DCs and IFN-α production, was consistent with their findings. Moreover, as Rutz et al. (35) have demonstrated that TLR9–CpG ODN interaction occurs at the acidic pH (6.5–5.0) found in early endosomes and lysosomes but not at physiological pH (7.4), the Hsp90-mediated translocation of CpG-ODNs into static early endosomes (pH 6.5) might accelerate the TLR9 and CpG–ODN interaction. In contrast, CpG-A alone, which did not stimulate IFN-α production, targeted the EEA1$^-$ and LAMP1$^+$ dynamic early endosome-late endosome/lysosome pathway, leading to inflammatory cytokine responses as well as DC maturation through NF-κB–mediated signaling. These data suggested that Hsp90 shuttled the chaperoned DNA into the static early endosome, resulting in the formation of DNA aggregation under mildly acidic circumstances as well as preventing translocation to late endosomes/lysosomes. Therefore, we hypothesized that targeting of DNA to static early endosomes was critical for eliciting TLR9 signaling for IFN-α production by DCs. Furthermore, we examined whether Hsp90 could convert CpG-B, which is thought to stimulate TLR9 in late endosomes, into a ligand that triggers TLR9 in early endosomes. Indeed, when complexed with Hsp90, CpG-B induced pDCs to produce high levels of IFN-α of pDCs and only low levels of IL-6 and TNF-α as compared with CpG-B alone; the Hsp90 complexed with CpG-B also failed to induce pDC maturation as revealed by the low surface expression of CD80 and CD86. These data suggested that the CpG-B–Hsp90 complex made possible their retention in early endosomes and subsequent induction of higher levels of IFN-α and low levels of IL-6 and TNF-α and impaired pDC maturation.

Recently, it has been demonstrated that pDCs do sense and respond to self-DNA in human autoimmune diseases. In systemic lupus erythematosus (SLE), pDCs are activated to produce IFNs by circulating immune complexes consisting of autoantibodies and self-nucleic acids that stimulate endosomal TLR following FcγRII-mediated uptake. The aberrantly produced IFNs are major effectors in the pathogenesis of autoimmunity, mainly by inducing unabated maturation of peripheral mDCs that stimulate autoreactive T cells. Recent evidence implies that upon internalization of chromatin–IgG immune complexes via BCR or FcRIII of DCs, mammalian DNA displays robust immunostimulatory activities toward B cells or DCs (36, 37). Furthermore, the sera of patients with SLE containing immune complexes consisting of autologous DNA and anti-DNA Abs effectively activate pDCs to produce type I IFNs (38, 39). We have demonstrated that, upon Hsp90-mediated enforced endosomal translocation, both human self-DNA as well as CpG-ODN could activate DCs via TLR9 to produce type I IFN. Previous studies have demonstrated the presence of autoantibodies to the Hsp90 (40, 41) and enhanced expression of Hsp90 in PBMCs of patients with active SLE (42, 43), suggesting the role of Hsp90 in the pathogenesis. In addition, the Hsp90 has been shown to localize both in the cytoplasm and nucleus (44). Moreover, under stressful conditions, it has been shown that cytosolic Hsp90 translocates to the nucleus (45). This suggests that Hsp90 may bind self-DNA within the nucleus. When cells undergo necrosis, self-DNA associated with endogenous Hsp90 could be released into the extracellular space and might trigger IFN-α production by pDCs. Our findings support the idea that Hsp90, an endogenous danger signal found in the sera from patients with SLE, is the key mediator of pDC activation in SLE. Thus, Hsp90 may inactivate innate tolerance to self-DNA by forming a complex with self-DNA that is delivered to and retained within early endocytic compartments of pDCs to trigger TLR9 and induce IFN production. Thus, we determined a fundamental mechanism by which pDCs sense and respond to self-DNA coupled with Hsp90. Our data suggest that, through this pathway, pDCs drive autoimmunity in autoimmune diseases.

The release of host-derived (self) DNA into the extracellular environment is a common feature of both necrotic and apoptotic cell death (46). However, extracellular self-DNA usually does not lead to innate immune activation because it is rapidly degraded by DNase and fails to access endosomal compartments of DCs where TLR9 is located. The importance of this mechanism in preventing autoimmune responses is shown by the fact that mice deficient in DNase 1 develop an SLE-like syndrome. Several host factors that can convert self-DNA into a trigger of DC activation have been reported. Endogenous anti-microbial peptide LL37 (also known as CAMP), autoantibodies, and high mobility group box 1 protein have been demonstrated to do so. In this study, we found that extracellular self-DNA acquires the ability to trigger activation of TLR9 in human pDC by forming a complex with the host-derived endogenous Hsp90.

Together, our findings indicate that the ability of Hsp90 to convert self-DNA into a trigger of high levels of IFN-α production depends on its capacity to concentrate and retain DNA in static early endosomes, presumably enabling the selective and sustained activation of early endosomal TLR9.

Acknowledgments

We thank Dr. S. Akira for providing *Tlr9*$^{-/-}$ mice.

Disclosures

The authors have no financial conflicts of interest.

References

1. Udono, H., and P. K. Srivastava. 1994. Comparison of tumor-specific immunogenicities of stress-induced proteins gp96, hsp90, and hsp70. *J. Immunol.* 152: 5398–5403.
2. Tamura, Y., P. Peng, K. Liu, M. Daou, and P. K. Srivastava. 1997. Immunotherapy of tumors with autologous tumor-derived heat shock protein preparations. *Science* 278: 117–120.
3. Sato, K., Y. Torimoto, Y. Tamura, M. Shindo, H. Shinzaki, K. Hirai, and Y. Kohgo. 2001. Immunotherapy using heat-shock protein preparations of leukemia cells after syngeneic bone marrow transplantation in mice. *Blood* 98: 1852–1857.
4. Milani, V., E. Noessner, S. Ghose, M. Kuppner, B. Ahrens, A. Scharner, R. Gastpar, and R. D. Issels. 2002. Heat shock protein 70: role in antigen presentation and immune stimulation. *Int. J. Hyperthermia* 18: 563–575.
5. Noessner, E., R. Gastpar, V. Milani, A. Brandl, P. J. Hutzler, M. C. Kuppner, M. Roos, E. Kremmer, A. Asea, S. K. Calderwood, and R. D. Issels. 2002. Tumor-derived heat shock protein 70 peptide complexes are cross-presented by human dendritic cells. *J. Immunol.* 169: 5424–5432.
6. Ueda, G., Y. Tamura, I. Hirai, K. Kamiguchi, S. Ichimiya, T. Torigoe, H. Hiratsuka, H. Sunakawa, and N. Sato. 2004. Tumor-derived heat shock protein 70-pulsed dendritic cells elicit tumor-specific cytotoxic T lymphocytes (CTLs) and tumor immunity. *Cancer Sci.* 95: 248–253.
7. Kurotaki, T., Y. Tamura, G. Ueda, J. Oura, G. Kutomi, Y. Hirohashi, H. Sahara, T. Torigoe, H. Hiratsuka, H. Sunakawa, et al. 2007. Efficient cross-presentation by heat shock protein 90-peptide complex-loaded dendritic cells via an endosomal pathway. *J. Immunol.* 179: 1803–1813.
8. Kutomi, G., Y. Tamura, K. Okuya, T. Yamamoto, Y. Hirohashi, K. Kamiguchi, J. Oura, K. Saito, T. Torigoe, S. Ogawa, et al. 2009. Targeting to static endosome is required for efficient cross-presentation of endoplasmic reticulum-resident oxygen-regulated protein 150-peptide complexes. *J. Immunol.* 183: 5861–5869.
9. Wagner, H. 1999. Bacterial CpG DNA activates immune cells to signal infectious danger. *Adv. Immunol.* 73: 329–368.
10. Krieg, A. M. 2002. CpG motifs in bacterial DNA and their immune effects. *Annu. Rev. Immunol.* 20: 709–760.
11. Ahmad-Nejad, P., H. Häcker, M. Rutz, S. Bauer, R. M. Vabulas, and H. Wagner. 2002. Bacterial CpG-DNA and lipopolysaccharides activate Toll-like receptors at distinct cellular compartments. *Eur. J. Immunol.* 32: 1958–1968.

12. Heil, F., P. Ahmad-Nejad, H. Hemmi, H. Hochrein, F. Ampenberger, T. Gellert, H. Dietrich, G. Lipford, K. Takeda, S. Akira, et al. 2003. The Toll-like receptor 7 (TLR7)-specific stimulus loxoribine uncovers a strong relationship within the TLR7, 8 and 9 subfamily. *Eur. J. Immunol.* 33: 2987–2997.
13. Lee, J., T. H. Chuang, V. Redecke, L. She, P. M. Pitha, D. A. Carson, E. Raz, and H. B. Cottam. 2003. Molecular basis for the immunostimulatory activity of guanine nucleoside analogs: activation of Toll-like receptor 7. *Proc. Natl. Acad. Sci. USA* 100: 6646–6651.
14. Matsumoto, M., K. Funami, M. Tanabe, H. Oshiumi, M. Shingai, Y. Seto, A. Yamamoto, and T. Seya. 2003. Subcellular localization of Toll-like receptor 3 in human dendritic cells. *J. Immunol.* 171: 3154–3162.
15. Latz, E., A. Schoenemeyer, A. Visintin, K. A. Fitzgerald, B. G. Monks, C. F. Knetter, E. Lien, N. J. Nilsen, T. Espevik, and D. T. Golenbock. 2004. TLR9 signals after translocating from the ER to CpG DNA in the lysosome. *Nat. Immunol.* 5: 190–198.
16. Honda, K., H. Yanai, H. Negishi, M. Asagiri, M. Sato, T. Mizutani, N. Shimada, Y. Ohba, A. Takaoka, N. Yoshida, and T. Taniguchi. 2005. IRF-7 is the master regulator of type-I interferon-dependent immune responses. *Nature* 434: 772–777.
17. Honda, K., Y. Ohba, H. Yanai, H. Negishi, T. Mizutani, A. Takaoka, C. Taya, and T. Taniguchi. 2005. Spatiotemporal regulation of MyD88-IRF-7 signalling for robust type-I interferon induction. *Nature* 434: 1035–1040.
18. Shortman, K., and Y. J. Liu. 2002. Mouse and human dendritic cell subtypes. *Nat. Rev. Immunol.* 2: 151–161.
19. Asselin-Paturel, C., A. Boonstra, M. Dalod, I. Durand, N. Yessaad, C. Dezutter-Dambuyant, A. Vicari, A. O'Garra, C. Biron, F. Brière, and G. Trinchieri. 2001. Mouse type I IFN-producing cells are immature APCs with plasmacytoid morphology. *Nat. Immunol.* 2: 1144–1150.
20. Nakano, H., M. Yanagita, and M. D. Gunn. 2001. CD11c(+)B220(+)Gr-1(+) cells in mouse lymph nodes and spleen display characteristics of plasmacytoid dendritic cells. *J. Exp. Med.* 194: 1171–1178.
21. Björck, P. 2001. Isolation and characterization of plasmacytoid dendritic cells from Flt3 ligand and granulocyte-macrophage colony-stimulating factor-treated mice. *Blood* 98: 3520–3526.
22. Perussia, B., V. Fanning, and G. Trinchieri. 1985. A leukocyte subset bearing HLA-DR antigens is responsible for in vitro alpha interferon production in response to viruses. *Natural Immunity and Cell Growth Regulation* 4: 120–137.
23. Siegal, F. P., N. Kadowaki, M. Shodell, P. A. Fitzgerald-Bocarsly, K. Shah, S. Ho, S. Antonenko, and Y. J. Liu. 1999. The nature of the principal type 1 interferon-producing cells in human blood. *Science* 284: 1835–1837.
24. Kadowaki, N., S. Antonenko, and Y. J. Liu. 2001. Distinct CpG DNA and polyinosinic-polycytidylic acid double-stranded RNA, respectively, stimulate CD11c- type 2 dendritic cell precursors and CD11c+ dendritic cells to produce type I IFN. *J. Immunol.* 166: 2291–2295.
25. Lande, R., J. Gregorio, V. Facchinetti, B. Chatterjee, Y. H. Wang, B. Homey, W. Cao, Y. H. Wang, B. Su, F. O. Nestle, et al. 2007. Plasmacytoid dendritic cells sense self-DNA coupled with antimicrobial peptide. *Nature* 449: 564–569.
26. Yasuda, K., P. Yu, C. J. Kirschning, B. Schlatter, F. Schmitz, A. Heit, S. Bauer, H. Hochrein, and H. Wagner. 2005. Endosomal translocation of vertebrate DNA activates dendritic cells via TLR9-dependent and -independent pathways. *J. Immunol.* 174: 6129–6136.
27. Klinman, D. M. 2004. Immunotherapeutic uses of CpG oligodeoxynucleotides. *Nat. Rev. Immunol.* 4: 249–258.
28. Manegold, C., D. Gravenor, D. Woytowitz, J. Mezger, V. Hirsh, G. Albert, M. Al-Adhami, D. Readett, A. M. Krieg, and C. G. Leichman. 2008. Randomized phase II trial of a toll-like receptor 9 agonist oligodeoxynucleotide, PF-3512676, in combination with first-line taxane plus platinum chemotherapy for advanced-stage non-small-cell lung cancer. *J. Clin. Oncol.* 26: 3979–3986.
29. Fourcade, J., P. Kudela, P. A. Andrade Filho, B. Janjic, S. R. Land, C. Sander, A. Krieg, A. Donnenberg, H. Shen, J. M. Kirkwood, and H. M. Zarour. 2008. Immunization with analog peptide in combination with CpG and montanide expands tumor antigen-specific CD8+ T cells in melanoma patients. *J. Immunother.* 31: 781–791.
30. Seif, A. E., D. M. Barrett, M. Milone, V. I. Brown, S. A. Grupp, and G. S. Reid. 2009. Long-term protection from syngeneic acute lymphoblastic leukemia by CpG ODN-mediated stimulation of innate and adaptive immune responses. *Blood* 114: 2459–2466.
31. Lakadamyali, M., M. J. Rust, and X. Zhuang. 2006. Ligands for clathrin-mediated endocytosis are differentially sorted into distinct populations of early endosomes. *Cell* 124: 997–1009.
32. Bandholtz, L., Y. Guo, C. Palmberg, K. Mattsson, B. Ohlsson, A. High, J. Shabanowitz, D. F. Hunt, H. Jörnvall, H. Wigzell, et al. 2003. Hsp90 binds CpG oligonucleotides directly: implications for hsp90 as a missing link in CpG signaling and recognition. *Cell. Mol. Life Sci.* 60: 422–429.
33. Wagner, H. 2004. The immunobiology of the TLR9 subfamily. *Trends Immunol.* 25: 381–386.
34. Guiducci, C., G. Ott, J. H. Chan, E. Damon, C. Calacsan, T. Matray, K. D. Lee, R. L. Coffman, and F. J. Barrat. 2006. Properties regulating the nature of the plasmacytoid dendritic cell response to Toll-like receptor 9 activation. *J. Exp. Med.* 203: 1999–2008.
35. Rutz, M., J. Metzger, T. Gellert, P. Luppa, G. B. Lipford, H. Wagner, and S. Bauer. 2004. Toll-like receptor 9 binds single-stranded CpG-DNA in a sequence- and pH-dependent manner. *Eur. J. Immunol.* 34: 2541–2550.
36. Leadbetter, E. A., I. R. Rifkin, A. M. Hohlbaum, B. C. Beaudette, M. J. Shlomchik, and A. Marshak-Rothstein. 2002. Chromatin-IgG complexes activate B cells by dual engagement of IgM and Toll-like receptors. *Nature* 416: 603–607.
37. Boulé, M. W., C. Broughton, F. Mackay, S. Akira, A. Marshak-Rothstein, and I. R. Rifkin. 2004. Toll-like receptor 9-dependent and -independent dendritic cell activation by chromatin-immunoglobulin G complexes. *J. Exp. Med.* 199: 1631–1640.
38. Vallin, H., A. Perers, G. V. Alm, and L. Rönnblom. 1999. Anti-double-stranded DNA antibodies and immunostimulatory plasmid DNA in combination mimic the endogenous IFN-alpha inducer in systemic lupus erythematosus. *J. Immunol.* 163: 6306–6313.
39. Magnusson, M., S. Magnusson, H. Vallin, L. Rönnblom, and G. V. Alm. 2001. Importance of CpG dinucleotides in activation of natural IFN-alpha-producing cells by a lupus-related oligodeoxynucleotide. *Scand. J. Immunol.* 54: 543–550.
40. Minota, S., S. Koyasu, I. Yahara, and J. Winfield. 1988. Autoantibodies to the heat-shock protein hsp90 in systemic lupus erythematosus. *J. Clin. Invest.* 81: 106–109.
41. Conroy, S. E., G. B. Faulds, W. Williams, D. S. Latchman, and D. A. Isenberg. 1994. Detection of autoantibodies to the 90 kDa heat shock protein in systemic lupus erythematosus and other autoimmune diseases. *Br. J. Rheumatol.* 33: 923–926.
42. Twomey, B. M., V. B. Dhillon, S. McCallum, D. A. Isenberg, and D. S. Latchman. 1993. Elevated levels of the 90 kD heat shock protein in patients with systemic lupus erythematosus are dependent upon enhanced transcription of the hsp90 beta gene. *J. Autoimmun.* 6: 495–506.
43. Ripley, B. J., D. A. Isenberg, and D. S. Latchman. 2001. Elevated levels of the 90 kDa heat shock protein (hsp90) in SLE correlate with levels of IL-6 and autoantibodies to hsp90. *J. Autoimmun.* 17: 341–346.
44. Perdew, G. H., N. Hord, C. E. Hollenback, and M. J. Welsh. 1993. Localization and characterization of the 86- and 84-kDa heat shock proteins in Hepa 1c1c7 cells. *Exp. Cell Res.* 209: 350–356.
45. Akner, G., K. Mossberg, K. G. Sundqvist, J. A. Gustafsson, and A. C. Wikström. 1992. Evidence for reversible, non-microtubule and non-microfilament-dependent nuclear translocation of hsp90 after heat shock in human fibroblasts. *Eur. J. Cell Biol.* 58: 356–364.
46. Pisetsky, D. S., and A. M. Fairhurst. 2007. The origin of extracellular DNA during the clearance of dead and dying cells. *Autoimmunity* 40: 281–284.

Cancer Science
The official journal of the Japanese Cancer Association

Melanoma-targeted chemo-thermo-immuno (CTI)-therapy using *N*-propionyl-4-*S*-cysteaminylphenol-magnetite nanoparticles elicits CTL response via heat shock protein-peptide complex release

Akiko Sato,[1] Yasuaki Tamura,[2,6] Noriyuki Sato,[2] Toshiharu Yamashita,[1] Tomoaki Takada,[1] Makito Sato,[1] Yasue Osai,[1] Masae Okura,[1] Ichiro Ono,[1] Akira Ito,[3] Hiroyuki Honda,[4] Kazumasa Wakamatsu,[5] Shosuke Ito[5] and Kowichi Jimbow[1]

Departments of [1]Dermatology and [2]Pathology, Sapporo Medical University, Sapporo; [3]Department of Chemical Engineering, Faculty of Engineering, Kyusyu University, Fukuoka; [4]Department of Biotechnology, Nagoya University, Nagoya; [5]Department of Chemistry, Fujita Health University, Toyoake, Japan

(Received February 1, 2010/Revised April 22, 2010/Accepted May 4, 2010/Accepted manuscript online May 19, 2010/Article first published online June 28, 2010)

Melanogenesis substrate, *N*-propionyl-4-*S*-cysteaminylphenol (NPrCAP) is specifically taken up by melanoma cells and inhibits their growth by producing cytotxic free radicals. By taking advantage of this unique chemical agent, we have established melanoma-targeting intracellular hyperthermia by conjugating NPrCAP with magnetite nanoparticles (NPrCAP/M) upon exposure to an alternating magnetic field (AMF). This treatment causes cytotoxic reaction as well as heat shock responses, leading to elicitation of antitumor immune response, which was proved by tumor rechallenge test and CTL induction. We found the level of heat shock protein 72 (Hsp72) to be increased in the cell lysate and culture supernatant after intracellular hyperthermia. Melanoma-specific $CD8^+$ T-cell response to dendritic cells loaded with hyperthermia-treated tumor lysate was enhanced when compared with non-treated tumor lysate. When heat shock protein, particularly Hsp72, was immuno-depleted from hyperthermia-treated tumor cell lysate, specific $CD8^+$ T-cell response was abolished. Thus, it is suggested that antitumor immune response induced by hyperthermia using NPrCAP/M is derived from the release of HSP-peptide complex from degraded tumor cells. Therefore, this chemo-thermo-immuno (CTI)-therapy might be effective not only for primary melanoma but also for distant metastasis because of induction of systemic antimelanoma immune responses. (*Cancer Sci* 2010; 101: 1939–1946)

Melanoma has been increasing in incidence leading to a rise in morbidity and mortality in recent decades. Metastatic melanoma is extremely difficult to cure and continues to have a poor prognosis. Only 12% with metastatic melanoma survive for 5 years.[1] The reason for this poor prognosis is the lack of effective conventional therapies. Various types of therapies such as immunotherapy, chemotherapy, and biologic therapy have been studied in melanoma management. However, a very modest effect was recorded in advanced malignant melanoma. Therefore, there is an emerging need for innovative therapies for the control of advanced melanoma.

It has been reported that the intracellular hyperthermia using magnetic nanoparticles is effective for treating certain types of cancer in not only primary but also metastatic lesions.[2–8] Incorporated magnetic nanoparticles generate heat within the cells after exposure to the alternating magnetic field (AMF) due to hysteresis loss or relaxational loss.[9,10] One of us has shown that hyperthermic treatment using magnetite cationic liposomes (MCLs), which are cationic liposomes containing 10-nm magnetite nanoparticles, induces antitumor immunity by enhancement of heat shock protein (HSP) expression.[3,11–13] We previously proposed that cross-presentation of extracellular HSP-peptide complex released from hyperthermia-induced necrotic tumor cells is the mechanism for inducing antitumor immunity.[7] In this paper, we present evidence that tumor-derived HSP-peptide complex is responsible for the hyperthermia-mediated antitumor immunity.

In addition, exploitation of biological properties unique to melanoma cells may provide a novel approach to improve the effect of hyperthermic treatment. We have previously shown that the sulfur-amine analog of tyrosine, 4-S-cysteaminyl phenol (4-*S*-CAP), and its *N*-acetyl or propionyl derivatives (NAcCAP or NPrCAP) are good substrates for melanoma-specific targeting and therapy. They have been shown to cause selective cytotoxicity against melanocytes and melanoma cells after selective uptake. Therefore, they can be good candidates for developing antimelanoma chemotherapy because melanogenesis is inherently toxic and expressed uniquely in melanocytic cells.[14–17] Recently, we synthesized new magnetite nanoparticles, NPrCAP/M, on which NPrCAP was directly conjugated on the surface of magnetite nanoparticles.[18,19] We have shown that NPrCAP/M is specifically targeted to melanoma cells, and internalized and aggregated within their cell cytoplasm. In addition, we have observed that B16 melanoma cells, which were subjected to intracellular hyperthermia using NPrCAP/M with AMF exposure, were brought to necrotic cell death, resulting in tumor growth retardation.[18] Here we show that the intracellular hyperthermic treatment using NPrCAP/M with AMF exposure induces tumor-specific immune responses and therefore we call this antimelanoma therapy ''chemo-thermo-immuno (CTI)'' therapy. We demonstrate that CTI therapy-induced antimelanoma immunity is mediated through cross-presentation of up-regulated intracellular and extracellular HSPs-peptide complex derived from melanoma cells.

Materials and Methods

Mice and cells. Female C57BL/6 mice were obtained from Hokudo (Sapporo, Japan) and used at 4–6 weeks of age.

[6]To whom correspondence should be addressed.
E-mail: ytamura@sapmed.ac.jp

doi: 10.1111/j.1349-7006.2010.01623.x

B16-OVA is a B16F1 melanoma cells stably transfected with chicken ovalbumin (OVA) cDNA (kindly provided by Dr Y. Nishimura, Kumamoto University, Kumamoto, Japan). B16-OVA was cultured in DMEM supplemented 10% FCS and 250 μg/mL of hygromycin B. B3Z is a $CD8^+$ T-cell hybridoma that expresses LacZ in response to activation of T-cell receptors specific for the SIINFEKL peptide (SL8; OVA-immunodominant peptide) in the context of $H\text{-}2K^b$ (kindly provided by Dr N. Shastri, University of California, Berkeley, CA, USA). B16F1 melanoma cells, CT26 colon carcinoma cells, and LLC lung carcinoma cells were cultured in DMEM supplemented with 10% FCS. EL4 lymphoma cells, YAC-1 cells, and B3Z cells were cultured in complete RPMI supplemented with 10% FCS. Bone marrow-derived dendritic cells (DCs) were generated from the femurs and tibiae of C57BL/6 mice. The bone marrow was flushed out, and the leukocytes were obtained and cultured in complete RPMI-1640 with 10% FCS and 20 ng/mL GM-CSF (Endogen, Woburn, MA, USA) for 5 days. On day 3, fresh medium with GM-CSF was added to the plates for the day 5 cultures.

Preparation of NPrCAP/M. Magnetite nanoparticles (Fe_3O_4; average particle size, 10 nm) were kindly provided by Toda Kogyo (Hiroshima, Japan). The details of the preparation of NPrCAP/M are described elsewhere.[18] Briefly, magnetite nanoparticles were coated with aminosilane and conjugated with NPrCAP via maleimide cross-linkers. The resultant NPrCAP/M was suspended in 10 mL of H_2O. The degree of incorporation of NPrCAP to magnetite was 61.0 nmol/mg magnetite.

Antibodies. For depletion of HSPs from cell lysate, anti-Hsp72/Hsc73 mAb, anti-Hsp90α polyclonal antibody, anti-Hsp90 mAb, and anti-lysine-aspartic acid-glutamic acid-leucine (KDEL) mAb were used. Anti-Hsp72/Hsc73 mAb and anti-Hsp90mAb were used for western blotting. These antibodies were obtained from StressGen Biotechnologies Victoria, BC, Canada). Mouse IgG and Rabbit IgG were purchased from IBL (Takasaki, Japan).

Measurement of iron concentration in the NPrCAP/M-exposed cells. Subconfluently growing melanoma and non-melanoma cells ($8 \times 10^4/cm^2$) in a 25-cm^2 flask were re-fed with the medium containing 5.94 mg of NPrCAP/M or magnetite (84 mg/mL). To discriminate between incorporation of NPrCAP/M and magnetite by direct attachment to cells and that by diffusion from the medium, culture flasks were fixed on a slanted disc and rotated slowly for 30 min. After the cells were washed with PBS twice and collected, they were dissolved completely in 200 μL of concentrated HCl and incubated at 43°C for 30 min. Then, 10 mL of H_2O_2 and 4 mL of 1% potassium thiocyanate were added in sequence to the cell solution. The concentration of NPrCAP/M used in these experiments was 24.4 μM as NPrCAP.

Transplantation of tumor cells and intracellular hyperthermia. All of the animal experiments were conducted with the approval of the Animal Experiment Ethics Committee of Sapporo Medical University. B16-OVA cells (1×10^6) were subcutaneously transplanted into the right flank of C57BL/6 mice on day 0. NPrCAP/M nanoparticles (24.4 μM as NPrCAP, 100 μL) were injected subcutaneously into the tumor on days 7, 9, 11, and 13. A magnetic field was created using a horizontal coil (inner diameter, 7 cm; length, 7 cm) with a transistor inverter (LTG-100-05; Dai-ichi High Frequency, Tokyo, Japan).[4] The magnetic field frequency and intensity were 118 KHz and 30.6 KA/m (386 Oe), respectively. Twenty-four hours after injection, mice were subjected to AMF exposure to heat the tumor at 43°C for 30 min. The heated field was three dimensions, which was created using a horizontal coil with a transistor inverter. The mice whose tumors were injected with NPrCAP/M were put in a horizontal coil and exposed to AMF. Moreover, we monitored the temperature of the tumor surface as well as the rectal temperature using an optical fiber probe. The temperature of the tumor surface was maintained at 43°C and rectal temperature was about 38°C. Tumor growth was recorded once every 2 days. The cured mice were then rechallenged with a subcutaneous injection of B16-OVA cells (1×10^6) or irrelevant 3LL lung carcinoma cells (1×10^6) on the left flank. Tumor size was determined by the following formula: tumor volume = $0.5 \times (\text{length} \times \text{width}^2)$, where length and width were measured in millimeters.

Histopathology of tumor sections. Twenty-one days after tumor challenge, subcutaneous B16-OVA tumors were harvested and fixed in 10% formalin in PBS, then paraffin embedded and sectioned. Hematoxylin–eosin (H&E)-stained sections were prepared for analysis of therapeutic effect and gross infiltrate. For immunohistochemical analysis, the frozen tissues were stained with an antimouse CD4 mAb (Santa Cruz Biotechnology, Santa Cruz, CA, USA) or an antimouse CD8 mAb (Chemicon International, Temecula, CA, USA) and then incubated with HRP-conjugated goat antirat Ig (Dako, Tokyo, Japan), followed by hematoxylin counterstaining.

***In vitro* cytotoxicity assay.** After mice were treated by intracellular hyperthermia as described above, spleens were harvested on day 28, then 5×10^6 spleen cells were restimulated *in vitro* with irradiated B16-OVA cells in 2 mL of RPMI-1640 supplemented with 50 μM of β-mercaptethanol (Invitrogen, Carlsbad, CA, USA) and 10% FCS for 5 days. Cytotoxic activity of the effector cells against target cells (B16-OVA, EL4, EL4 loaded with SL8 peptide and YAC-1) was determined by standard ^{51}Cr release assay.

Quantification of HSPs. Cultured B16-OVA cells were exposed to NPrCAP/M for 30 min and irradiated by AMF to heat them at 43°C. After NPrCAP/M exposure with or without AMF irradiation, cells (1×10^6) were cultured in 1 mL of 10% RPMI for 72 h. Culture supernatant was collected at 12, 24, and 48 h, or cells escaping cell death were lysed at 72 h after intracellular hyperthermia by freezing and thawing and centrifugation at 2380 *g* for 5 min. The expression of Hsp72/Hsc73 and Hsp90 was determined by western blotting with an anti-Hsp72/Hsc73 mAb or anti-Hsp90 mAb. Heat shock protein (HSP) in the lysate or culture supernatant was quantified by the Hsp90α ELISA and Hsp70 ELISA kits (StressGen), which can detect and quantify Hsp90α and inducible Hsp72, respectively.

Cross-presentation of antigen derived from hyperthermia-treated tumor cell lysate by DCs. Cultured B16-OVA cells were exposed to NPrCAP/M for 30 min and irradiated by AMF to heat them at 43°C. After NPrCAP/M exposure with or without AMF irradiation, cells were cultured for 72 h and 1×10^7 of cells in 1 mL of 10% RPMI medium were lysed by three cycles of freezing and thawing and centrifugation at 2380*g* for 5 min. Dendritic cells DCs (1×10^5) derived from bone marrow of C57BL/6 mice were pulsed with the cell lysate (100 μL) and incubated with 1×10^5 B3Z T cell hybridoma. After overnight incubation, LacZ activity was measured by addition of 100 μL of chlorophenol red-β-D-galactopyranoside (CPRG, Roche, Basel, Switzerland) solution. The absorbance was measured at 595 nm after 4-h incubation at 37°C.

Immunodepletion of HSP. Cultured B16-OVA cells were treated and lysed as described above. The cell lysate (100 μL) was incubated with antibodies (5 μg each) against Hsp90, Hsp72/Hsc73, KDEL, or all of them. The mixture was added to 10 μL of protein A-Sepharose beads (50% slurry; GE Healthcare Japan, Tokyo, Japan), and the suspension was rotated at RT for 1 h. Then, the suspension was spun at 14 000*g* for 1 min. After removal of the beads, the supernatant was used for cross-presentation assay using B3Z as described above. Mouse IgG (15 μg) was used as an experimental control. Depletion was assessed by immunoblotting with anti-Hsp90, Hsp72/Hsc73, or KDEL antibodies.

doi: 10.1111/j.1349-7006.2010.01623.x

***In vivo* cross-presentation of antigen derived from melanoma cells after CTI therapy.** B16-OVA cells (1×10^6) were transplanted into the footpads of C57BL/6 mice on day 0. NPrCAP/M nanoparticles (24.4 μM as NPrCAP, 100 μL) were injected into the tumor on days 7, 9, 11, and 13. Twenty-four hours after injection, mice were subjected to AMF exposure to heat the tumor at 43°C for 30 min. Control mice were injected with PBS or NPrCAP/M nanoparticles alone without hyperthermia. After 5 h of the last CTI therapy against B16-OVA, popliteal nodes were removed and DCs were isolated using CD11c MACS beads (Miltenyi Biotec).Then, B3Z cells (1×10^5) were added to the DC culture (1×10^5) in 96-well flat-bottom plates and incubated at 37°C. Twenty-four hours after incubation, absorbance at 595 nm was measured.

Statistical analyses. All experiments were independently performed three times in triplicate. Comparisons between two groups were performed using Student's *t*-test. In the tumor transplantation assay, we determined statistical significance using Kruskal–Wallis one-way analysis. In all experiments, differences were considered statistically significant at $P < 0.05$.

Results

***N*-propionyl-4-*S*-cysteaminylphenol with magnetite nanoparticles (NPrCAP/M) was preferentially incorporated into melanoma cells.** To examine whether NPrCAP/M could be incorporated into melanoma cells more preferentially than magnetite alone, we compared amounts of iron molecules in cells after culture in the NPrCAP/M- or magnetite-containing media. As shown in Figure 1, B16F1, B16-OVA melanoma cells incorporated large amounts of iron derived from NPrCAP/M compared to that from magnetite alone. Non-melanoma CT26 colon carcinoma and LLC lung carcinoma cells captured a small amount of NPrCAP/M; however, the amount was not significantly different from that with magnetite alone or was almost the same as for magnetite. These data suggested that NPrCAP/M nanoparticle was an ideal agent for specific targeting to melanoma cells.

Antitumor effect of intracellular hyperthermia using NPrCAP/M with AMF exposure and its ability to induce antitumor immunity. We have recently reported the efficacy of melanoma growth inhibition by combination therapy of NPrCAP/M administration with AMF exposure.[19] B16F1 melanoma bearing mice treated with NPrCAP/M injection followed by hyperthermia showed apparent tumor growth retardation. In addition, we have observed that treatment with NPrCAP/M alone (without hyperthermia) also showed the growth suppression of B16F1 melanoma, indicating that NPrCAP/M has a chemotherapeutic effect. In this paper, we used B16-OVA, which was B16 melanoma transfected with OVA as a surrogate tumor antigen, to examine the antigen-specific antitumor immune response. Mice were transplanted with B16-OVA melanoma cells and treated with NPrCAP/M injection followed by hyperthermia or NPrCAP/M injection alone as described in the Materials and Methods. Histopathological examination of the day 21 tumors without treatment showed that inflammatory infiltrates were poorly detected including $CD8^+$ T cells and $CD4^+$ T cells (Fig. 2a-i, -ii, -iii, -iv). In contrast, treatment with combination of NPrCAP/M injection and hyperthermia induced apparent tumor destruction and necrosis with deposit of NPrCAP/M particles (Fig. 2a-v, -vi). In addition, a dense inflammatory infiltrate including neutrophiles, macrophages, plasma cells, and lymphocytes was observed around the residual tumor cells (Fig. 2a-vii, -viii). Furthermore, we have observed that this infiltrate included both $CD8^+$ T cells and $CD4^+$ T cells (Fig. 2a-ix, -x). These T cells were hardly seen around the tumor without treatment or with NPrCAP/M without AMF exposure (data not shown). Tumor volume in the group treated by combination of NPrCAP/M injection and hyperthermia was significantly reduced compared with the non-treated control group ($P = 0.0025$) and the group of NPrCAP alone ($P = 0.023$) (Fig. 2b). Six out of 10 mice in the group treated by NPrCAP/M injection and hyperthermia were cured. In contrast, all mice died of tumor burden in the treatment with NPrCAP/M without AMF and control groups. Interestingly, both NPrCAP/M with and without AMF exposure resulted in a significant and equal reduction of melanoma tumor volume by 17 days after tumor challenge. However, the tumors of mice treated with NPrCAP/M without AMF exposure grew rapidly after day 17. This suggested that hyperthermia might be required for the complete elimination of melanoma tumors. To examine whether cured mice developed antitumor immune responses, these mice were rechallenged with live B16-OVA melanoma cells or irrelevant mouse lung carcinoma LLC 4 weeks after NPrCAP/M and hyperthermic treatment. As a result, all cured mice rejected a rechallenge of live B16-OVA melanoma cells, but not LLC lung carcinoma cells (Fig. 2c). These data indicated that intracellular hyperthermia using NPrCAP/M with AMF exposure induced specific antitumor immunity.

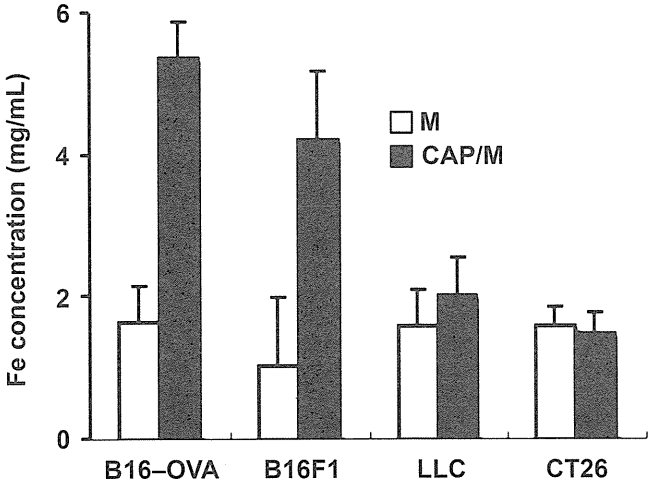

Fig. 1. *N*-propionyl-4-*S*-cysteaminylphenol with magnetite nanoparticles (NPrCAP/M) was preferentially incorporated into melanoma cells. Subconfluently growing melanoma and non-melanoma cells ($8 \times 104/cm^2$) in a 25 cm^2 flask were fed with medium containing 5.94 mg of NPrCAP/M or magnetite (84 mg/mL) for 30 min. Iron concentration of magnetite nanoparticles was measured using the potassium thiocyanate method.

Induction of tumor-specific CTL by intracellular hyperthermia. To analyze the mechanism for the generation of antitumor immunity by NPrCAP/M and hyperthermia, we examined CTL induction in mice after intracellular hyperthermia. Spleen cells of mice after hyperthermia showed high cytotoxicity against B16-OVA melanoma cells compared to EL4 lymphoma and YAC-1 cells. In addition, spleen cells also showed high cytotoxicity against EL4 pulsed with SL8 peptide derived from OVA protein (Fig. 3). These results suggest that intracellular hyperthermia using NPrCAP/M can elicit specific tumor immunity by inducing CTL against B16-OVA melanoma cells.

Enhanced expression of Hsp72 in B16-OVA melanoma cell after intracellular hyperthermia. We examined the expression of HSPs in tumor cells treated with NPrCAP with AMF exposure *in vitro* by western blotting and ELISA. The protein level of Hsp72 but not Hsc73 or Hsp90 was increased at 48 h after hyperthermia (Fig. 4a). Similarly, the concentration of Hsp72 in cell lysate resulted in a three-fold increase at 72 h after hyperthermia, compared to cells without treatment (Fig. 4b). However, the concentration of Hsp90 did not change (Fig. 4c).

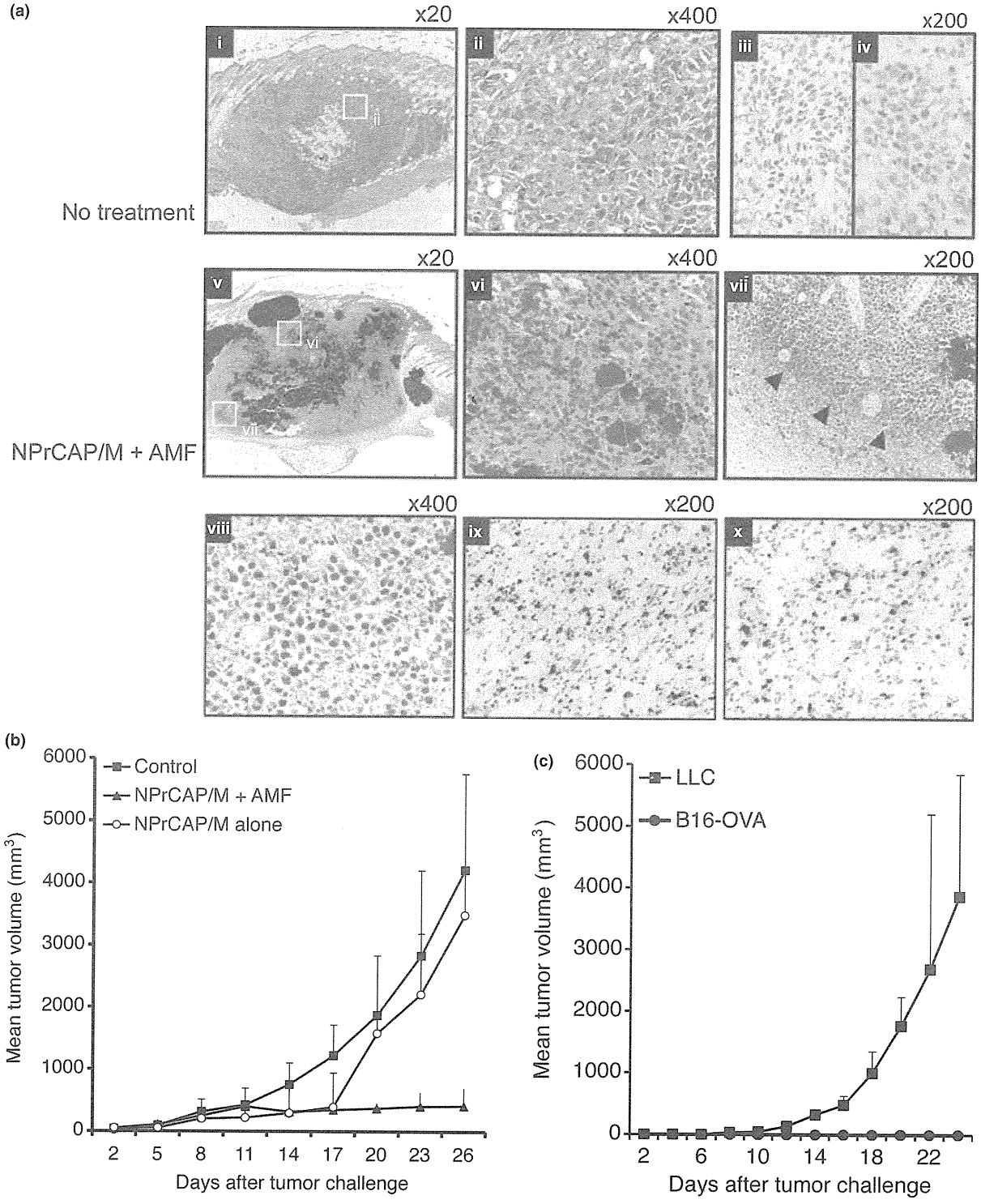

Fig. 2. Antitumor effect and tumor-specific immunity induced by intracellular hyperthermia using *N*-propionyl-4-*S*-cysteaminylphenol with magnetite nanoparticles (NPrCAP/M) and alternating magnetic field (AMF) exposure. (a) Pre-established subcutaneous B16-OVA tumors without treatment (i,ii,iii,iv) or intracellular hyperthermia using NPrCAP/M with AMF exposure (v,vi,vii,viii,ix,x) were harvested and analyzed histologically using H&E-stained sections. Intracellular hyperthermia using NPrCAP with AMF exposure induced tumor destruction and inflammatory infiltrate (arrow head). The frozen tissues excised from mice untreated or treated with NPrCAP/M with AMF exposure were stained with an antimouse CD8 mAb (iii,ix) or CD4 mAb (iv,x). (b) Tumor growth of B16-OVA melanoma cells in non-treated control mice (n = 10), mice treated with NPrCAP/M with AMF exposure (n = 10), or mice treated with NPrCAP/M alone (n = 10). Points, mean tumor volume (mm^3); bars, SD. (c) The development of tumor specific immunity by intracellular hyperthermia. Mice cured by intracellular hyperthermia were rechallenged with B16-OVA melanoma cells (n = 3) or lung carcinoma LLC (n = 3). Mice were transplanted with 1×10^6 B16-OVA cells and then the tumor growth rates of each group were compared using the average tumor size. Points, mean tumor volume (mm^3); bars, SD. Results shown are representative of three different experiments.

doi: 10.1111/j.1349-7006.2010.01623.x

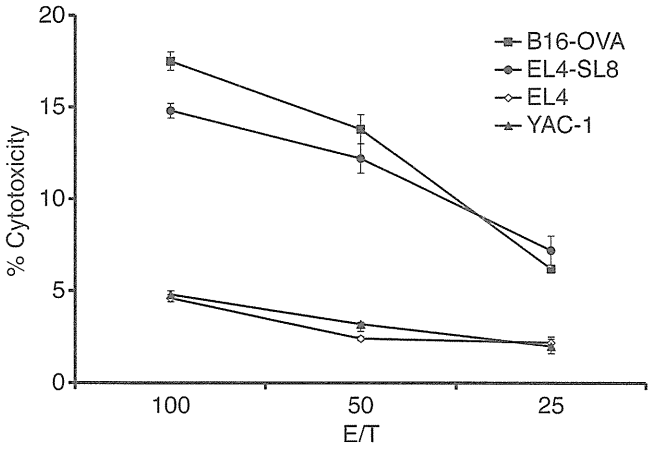

Fig. 3. Induction of tumor-specific CTL by intracellular hyperthermia. Analysis of spelenocytes cytotoxic activity against B16-OVA melanoma cells, EL4, EL4 pulsed with SL8 peptide, and YAC-1 in ^{51}Cr release assay. Mice were treated by *N*-propionyl-4-*S*-cysteaminylphenol with magnetite nanoparticles (NPrCAP/M) injection followed by alternating magnetic field (AMF) exposure. Four weeks after treatment, spleen cells were removed and stimulated with irradiated B16-OVA cells. Cytotoxic activity of spleen cells against B16-OVA cells, EL4 cells, EL4 cells pulsed with SL8 peptide, or YAC-1 cells was determined by standard ^{51}Cr-release assay. Bars, SD.

Treatment with NPrCAP alone decreased the level of intracellular Hsp72 and Hsp90. We are currently investigating the underlying mechanism. From the results obtained, we hypothesized that hyperthermia using NPrCAP/M might induce tumor immunity through up-regulation of Hsp72.

Intracellular hyperthermia using NPrCAP/M with AMF exposure results in the release of HSPs into the extracellular milieu. It has been demonstrated that once cancer cells become necrotic, several HSPs, above all, Hsp72 and Hsp90, are released from cells and might act as a danger signal, subsequently eliciting cell-specific immune responses. We therefore examined whether Hsp72 and Hsp90 would be released from necrotic melanoma cells after intracellular hyperthermia *in vitro*. Culture supernatants from B16-OVA were collected at 12, 24, and 48 h after intracellular hyperthermia and the quantity of Hsp72 and Hsp90 was evaluated using ELISA. Although Hsp72 and Hsp90 were detected at 48 h after hyperthermia, concentration of extracellular Hsp72 was a 4.5-fold higher than that of Hsp90 (Fig. 4d). These *in vitro* results suggested that treatment of B16-OVA melanoma with intracellular hyperthermia would release HSPs, in particular Hsp72, into extracellular milieu *in vivo* and these extracellular HSPs might play an important role in inducing antitumor immunity.

$CD8^+$ T-cell response against DCs loaded with B16-OVA melanoma cell lysate after intracellular hyperthermia. To analyze the mechanism of tumor specific CTL induction, we examined B3Z $CD8^+$ T-cell response against DCs loaded with supernatant from B16-OVA culture after intracellular hyperthermia. However, only a very modest response was observed (data not shown). One of the reasons for this modest response may be the degradation of peptide chaperoned by HSPs by protease in the culture medium. We therefore decided to use melanoma cell lysate after hyperthermia. NPrCAP/M loaded B16-OVA melanoma cells were subjected to AMF irradiation and cultured for 72 h. Melanoma cells were lysed by three cycles of freezing and thawing. Dendritic cells (DCs) derived from mouse bone marrow were loaded with the lysate for 2 h and then cultured with B3Z $CD8^+$ T-cell hybridoma. B3Z response against DC loaded with B16-OVA melanoma cell lysate increased after intracellular hyperthermia using NPrCAP/M, compared with non-heated cells and cells loaded NPrCAP/M without AMF exposure (Fig. 5a). These data demonstrated that loading DCs with lysate derived from melanoma cells treated with hyperthermia enhanced the cross-presentation of B16-OVA-specific antigen peptide.

Effects of immunodepletion of HSPs on $CD8^+$ T-cell response. Next, we investigated the underlying mechanism

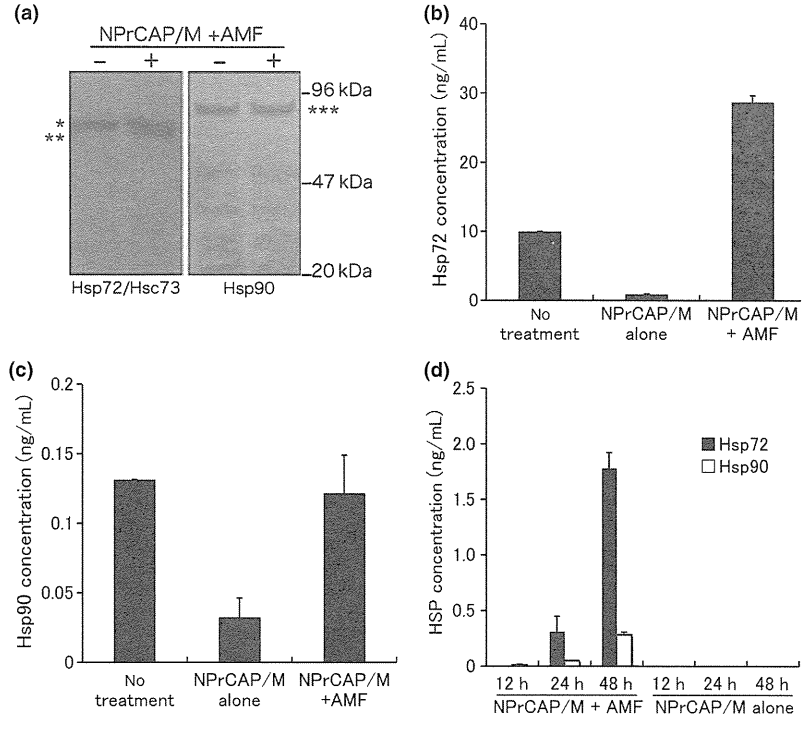

Fig. 4. Heat shock protein (HSP) expression in tumor cells after intracellular hyperthermia. (a–c) B16-OVA cells were subjected to hyperthermia using *N*-propionyl-4-*S*-cysteaminylphenol with magnetite nanoparticles (NPrCAP/M) with alternating magnetic field (AMF) exposure *in vitro*. Seventy-two hours after intracellular hyperthermia (+) or left untreated (–), the expression of Hsp72 and Hsp90 was determined by western blotting with an anti-Hsp72/Hsc73 mAb or anti-Hsp90 mAb (a). *Hsc73, **Hsp72, ***Hsp90. The expression of Hsp72 was markedly enhanced by intracellular hyperthermia. Heat shock protein (HSP) in the lysate was quantified by the Hsp72 ELISA (b) and Hsp90 ELISA kits (c). (d) Hsp72 and Hsp90 in the 12-, 24- and 48-h culture supernatant after intracellular hyperthermia were measured using ELISA. Bars, SD. Results shown are representative of three different experiments.

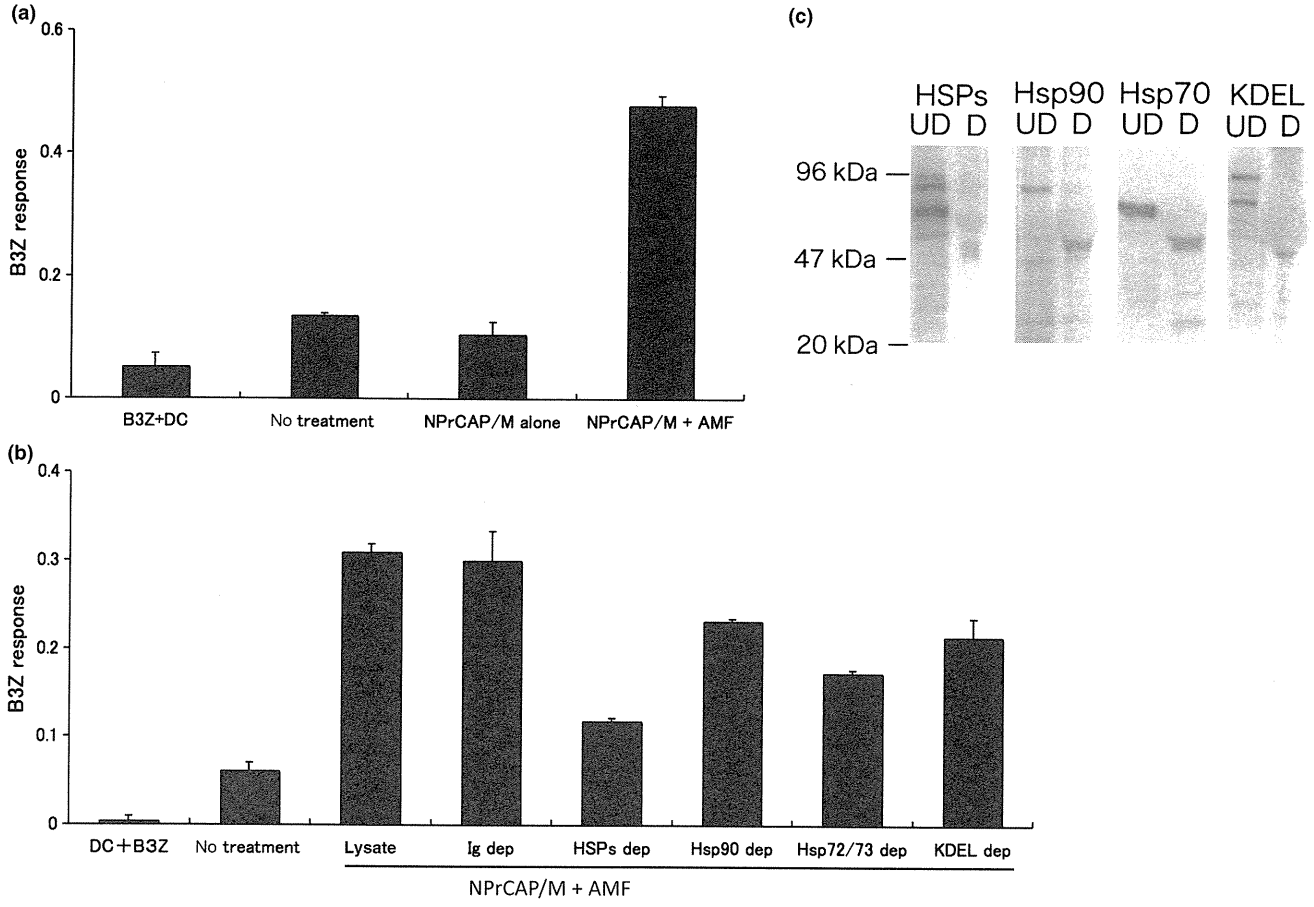

Fig. 5. $CD8^+$ T-cell response against dendritic cells (DCs) pulsed with B16-OVA melanoma cell lysate after intracellular hyperthermia and effect of heat shock protein (HSP) depletion. (a) B16-OVA cells were subjected to *N*-propionyl-4-*S*-cysteaminylphenol with magnetite nanoparticles (NPrCAP/M) exposure and alternating magnetic field (AMF) irradiation, then lysed by freezing and thawing. Dendritic cells (DCs) were pulsed with the cell lysate, and cultured overnight with B3Z and the absorbance of β-galactosidase activity was measured at 595 nm. Bars, SD. (b) Lysates of the cells were immunoprecipitated with anti-Hsp72/Hsc73 antibody, anti-Hsp90 antibody and anti-KDEL antibody. Immunoprecipitates were removed from lysate. After being pulsed with the HSP-depleted lysate, DCs were incubated with B3Z T cell hybridoma and the absorbance of β -galactosidase activity was measured at 595 nm. Bars, SD. (c) Cell lysates were depleted of HSPs (above lanes) with antibodies specific for each HSP. Immunoblots were of depleted (D) or undepleted (UD) lysates. Results shown are representative of five different experiments.

responsible for the enhancement of cross-presentation by intracellular hyperthermia. Hyperthermia has long been shown to induce the expression of HSPs within tumor cells, which have been shown to chaperone tumor-associated antigen peptides. To investigate the role of HSPs in intracellular hyperthermia-induced $CD8^+$ T-cell response, we depleted HSPs from lysate using anti-HSP antibody, and measured $CD8^+$ T-cell response against DCs loaded with the HSP-depleted lysate. Depletion of major HSPs (Hsp72/Hsc73, Hsp90, and ER-resident HSPs) from NPrCAP/M and hyperthermic treated B16-OVA cell lysate caused a loss of 59% of initial B3Z response ($P = 0.0001$ *vs* depletion with control Ig) (Fig. 5b), whereas depletion with control Ig did not show any effect. Importantly, depletion of Hsp72/Hsc73 exhibited a 44% reduction of activity and it was best decreased in response in the HSP depletion assay. The inhibition rate was statistically significant compared with the depletion with control Ig ($P = 0.001$). Depletion of Hsp90 or ER resident HSPs caused a loss of 25% ($P = 0.0857$) or 31% ($P = 0.0034$) of the initial activity, respectively. Immunoblots showed that depletion of each HSP was complete (Fig. 5c). These results suggested that Hsp72/Hsc73, Hsp90, and ER-resident HSPs were involved in the induction of CTL response at various extents. In addition, our data demonstrated that these HSPs chaperoned antigenic peptides and extracellular HSP-peptide complexes were cross-presented by DCs, followed by specific CTL activation. Notably, Hsp72/Hsc73 was largely responsible for the observed T-cell response. As shown in Figure 4, these data were consistent with the enhanced expression of Hsp72 within the melanoma cells. Thus, DCs loaded with intracellular hyperthermia-treated melanoma cell lysate are more efficient than DCs loaded with untreated melanoma cell lysate in cross-presentation to CTLs.

Dendritic cells (DCs) derived from tumor-draining lymph nodes cross-present melanoma-associated antigen after CTI therapy. We examined whether melanoma-associated antigen was indeed cross-presented by DCs within tumor-draining lymph nodes after CTI therapy. To test this, we transplanted B16 melanoma cells into the footpads of mice. After three rounds of CTI therapy, tumor-draining popliteal nodes were removed and DCs were isolated and cultured with B3Z. B3Z response against regional lymph node-derived DCs of CTI-treated mice was evident when compared to PBS control or NPrCAP/M injection without hyperthermia (Fig. 6). We therefore conclude that intracellular hyperthermia using NPrCAP/M with

doi: 10.1111/j.1349-7006.2010.01623.x

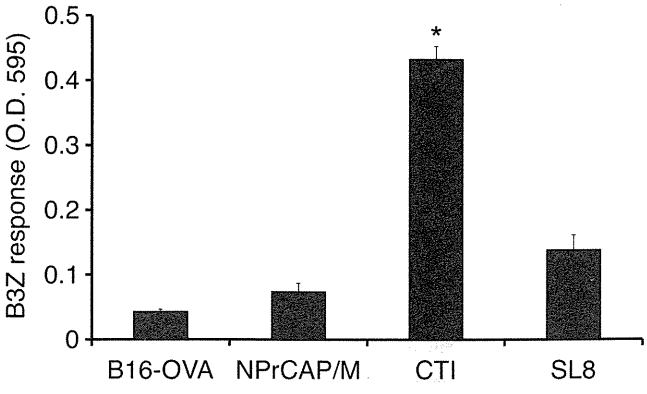

Fig. 6. Dendritic cells (DCs) derived from tumor-draining lymph nodes cross-present melanoma-associated antigen after CTI therapy. B16-OVA cells (1×10^6) were transplanted into the footpads of C57BL/6 mice on day 0. *N*-propionyl-4-*S*-cysteaminylphenol with magnetite nanoparticles (NPrCAP/M) nanoparticles (24.4 mM as NPrCAP, 100 mL) were injected into the tumor on days 7, 9, 11, and 13. Twenty-four hours after injection, mice were subjected to alternating magnetic field (AMF) exposure to heat the tumor at 43°C for 30 min. Control mice were injected with PBS or NPrCAP/M nanoparticles alone without hyperthermia. After 5 h of the last CTI therapy against B16-OVA, tumor-draining popliteal nodes were removed and DCs were isolated, then cultured with B3Z cells. Twenty-four hours after incubation, absorbance at 595 nm was measured. Bars, SD. $*P < 0.01$; paired Student's *t*-test. Data are representative of three independent experiments.

AMF exposure promotes OVA-derived peptide presentation on DCs both *in vitro* and *in vivo*.

Discussion

In this study, we showed that intracellular hyperthermia of melanoma cells using NPrCAP/M with AMF exposure elicited antitumor immune responses via cross-presentation of HSP-chaperoned antigen. Moreover, we demonstrated that DCs derived from tumor-draining lymph nodes indeed cross-presented melanoma-associated antigen after CTI therapy. It has been believed that enhanced expression of intracellular HSPs by hyperthermia plays an important role in the induction of antitumor immunity.[11,20] Moreover, it has been demonstrated that overexpression of HSPs, particularly Hsp72, causes increased tumor immunogenicity due to augmentation of the chaperoning ability of antigenic peptide, thereby augmenting the presentation of antigenic peptide in the context of MHC class I molecules.[21,22] However, in order to prime tumor-specific immunity, it is necessary to present tumor antigen in the context of MHC class I in conjunction with the co-stimulation signal through co-stimulatory molecules such as B7.1 and B7.2 by professional antigen-presenting cells such as DCs. Dendritic cells (DCs) have the unique capacity to take up, process, and present exogenous antigens in association with MHC class I molecules. This process is termed cross-presentation and the resulting $CD8^+$ T-cell priming is referred to as cross-priming. It has been demonstrated that some exogenous antigens such as HSPs[23–27] and particulate protein antigens[28] gain access to the MHC class I processing pathway and initiate CTL responses. This exogenous pathway is important for the development of $CD8^+$ CTL responses against tumors and infectious pathogens that do not have access to the classical MHC class I pathway.

Here, we showed that the HSPs-antigen peptide complex released from melanoma cells treated with intracellular hyperthermia is taken up by DCs and cross-presented HSP-chaperoned peptide in the context of MHC class I molecules (Fig. 7). Our CTI therapy induced NPrCAP- as well as heat-mediated melanoma cell necrosis to NPrCAP/M incorporated cells. We have reported that repeated hyperthermia (three cycles of NPrCAP/M injection and AMF irradiation) was required to induce the maximal antitumor immune responses.[19] If melanoma cells escape from necrotic cell death, repeated hyperthermia should produce necrotic cell death of previously heat shocked-melanoma cells in which HSPs were induced. In fact, our data suggested that Hsp72/Hsc73, Hsp90, and ER-resident

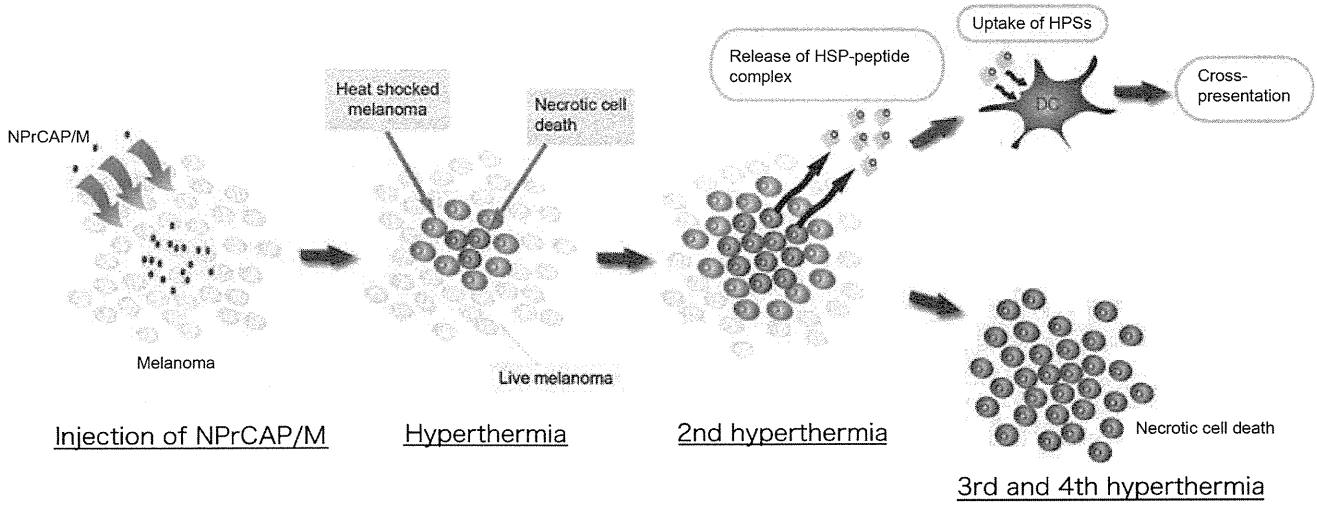

Fig. 7. Schema of intracellular hyperthermia using *N*-propionyl-4-*S*-cysteaminylphenol with magnetite nanoparticles (NPrCAP/M) with alternating magnetic field (AMF) exposure. Injected NPrCAP/M nanoparticles are specifically incorporated in melanoma cells. Intracellular hyperthermia can induce necrotic cell death and adjacent live melanoma cells suffer heat shock, resulting in increased level of intracellular heat shock protein (HSP)-peptide complexes. Repeated hyperthermia turns heat-shocked cells to necrotic cells, leading to the release of their intracellular contents, including HSPs-peptide complexes, into extracellular milieu. The released HSPs-peptide complexes are taken up by dendritic cells (DCs). Then, DCs migrate into regional lymph nodes and cross-present HSP-chaperoned antigenic peptides to $CD8^+$ T cells in the context of MHC class I molecules, thereby inducing antimelanoma CTLs. Finally, the remaining melanoma cells are killed by repeated hyperthermia or by the melanoma-specific CTLs.

HSPs participated in the induction of $CD8^+$ T-cell response. In particular, among HSPs, Hsp72 was largely responsible for the augmented antigen presentation to $CD8^+$ T cells. As Hsp72 is known to up-regulate in response to hyperthermia or heat shock treatment,[11] newly synthesized Hsp72 has a chance to bind to the heat-denatured melanoma-associated antigen.

Taken together, intracellular hyperthermia using NPrCAP/M is a promising treatment for improvement of clinical effects, especially for patients with advanced metastatic melanomas, and even for prevention of recurrence and/or metastasis for early melanomas because of induction of systemic antimelanoma immunity.

Acknowledgments

We thank Dr Shastri for providing B3Z T cell hybridoma, Dr Nishimura for providing B16-OVA, and Toda Kogyo Co. for providing the magnetite. This work was supported by a Health and Labor Sciences Research Grant-in-Aid for Research on Advanced Medical Technology from the Ministry of Health, Labor and Welfare of Japan.

Disclosure Statement

The authors have no conflict of interest.

References

1 Balch CM, Buzaid AC, Soong SJ *et al.* Final version of the American Joint Committee on Cancer staging system for cutaneous melanoma. *J Clin Oncol* 2001; **19**: 3635–48.
2 Yanase M, Shinkai M, Honda H, Wakabayashi T, Yoshida J, Kobayashi T. Intracellular hyperthermia for cancer using magnetite cationic liposomes: an in vivo study. *Jpn J Cancer Res* 1998; **89**: 463–9.
3 Kawai N, Ito A, Nakahara Y *et al.* Anticancer effect of hyperthermia on prostate cancer mediated by magnetite cationic liposomes and immune-response induction in transplanted syngeneic rats. *Prostate* 2005; **64**: 373–81.
4 Ito A, Shinkai M, Honda H, Kobayashi T. Medical application of functionalized magnetic nanoparticles. *J Biosci Bioeng* 2005; **100**: 1–11.
5 Yanase M, Shinkai M, Honda H, Wakabayashi T, Yoshida J, Kobayashi T. Antitumor immunity induction by intracellular hyperthermia using magnetite cationic liposomes. *Jpn J Cancer Res* 1998; **89**: 775–82.
6 Ito A, Shinkai M, Honda H, Wakabayashi T, Yoshida J, Kobayashi T. Augmentation of MHC class I antigen presentation via heat shock protein expression by hyperthermia. *Cancer Immunol Immunother* 2001; **50**: 515–22.
7 Ito A, Kobayashi T, Honda H. A mechanism of antitumor immunity induced by hyperthermia. *Jpn J Hyperthermic Oncol* 2005; **21**: 1–19.
8 Ito A, Takeshi K. Intracellular hyperthermia using magnetite nanoparticles: a novel method for hyperthermia clinical applications. *Thermal Medicine* 2008; **24**: 113–29.
9 Shinkai M, Yanase M, Honda H, Wakabayashi T, Yoshida J, Kobayashi T. Intracellular hyperthermia for cancer using magnetite cationic liposomes: in vitro study. *Jpn J Cancer Res* 1996; **87**: 1179–83.
10 Hergt R, Dutz S, Mueller R, Zeisberger M. Magnetite particle hyperthermia: nanoparticle magnetism and materials development for cancer therapy. *J Phys Condens Matter* 2006; **18**: S2919–34.
11 Ito A, Shinkai M, Honda H *et al.* Heat shock protein 70 expression induces antitumor immunity during intracellular hyperthermia using magnetite nanoparticles. *Cancer Immunol Immunother* 2003; **52**: 80–8.
12 Ito A, Matsuoka F, Honda H, Kobayashi T. Antitumor effects of combined therapy of recombinant heat shock protein 70 and hyperthermia using magnetic nanoparticles in an experimental subcutaneous murine melanoma. *Cancer Immunol Immunother* 2004; **53**: 26–32.
13 Ito A, Honda H, Kobayashi T. Cancer immunotherapy based on intracellular hyperthermia using magnetite nanoparticles: a novel concept of "heat-controlled necrosis" with heat shock protein expression. *Cancer Immunol Immunother* 2006; **55**: 320–8.
14 Ito Y, Jimbow K. Selective cytotoxicity of 4-S-cysteaminylphenol on follicular melanocytes of the black mouse: rational basis for its application to melanoma chemotherapy. *Cancer Res* 1987; **47**: 3278–84.
15 Miura S, Ueda T, Jimbow K, Ito S, Fujita K. Synthesis of cysteinylphenol, cysteaminylphenol, and related compounds, and in vivo evaluation of antimelanoma effect. *Arch Dermatol Res* 1987; **279**: 219–25.
16 Miura T, Jimbow K, Ito S. The in vivo antimelanoma effect of 4-S-cysteaminylphenol and its n-acetyl derivative. *Int J Cancer* 1990; **46**: 931–4.
17 Thomas PD, Kishi H, Cao H *et al.* Selective incorporation and specific cytocidal effect as the cellular basis for the antimelanoma action of sulphur containing tyrosine analogs. *J Invest Dermatol* 1999; **113**: 928–34.
18 Sato M, Yamashita T, Ohkura M *et al.* N-propionyl- cysteaminylphenol - magnetite conjugate (NPrCAP/M) is a nanoparticle for the targeted growth suppression of melanoma cells. *J Invest Dermatol* 2009; **129**: 2233–41.
19 Takada T, Yamashita T, Sato M *et al.* Growth inhibition of re-challenge B16 melanoma transplant by conjugates of melanogenesis substrate and magnetite nanoparticles as the basis for developing melanoma-targeted chemo-thermo-immunotherapy. *J Biomed Biotechnol* 2009; **2009**: 457936.
20 Mise K, Kan N, Okino T *et al.* Effect of heat treatment on tumor cells and antitumor effector cells. *Cancer Res* 1990; **50**: 6199–202.
21 Wells AD, Rai SK, Salvato MS, Band H, Malkovsky M. Hsp72-mediated augmentation of MHC class I surface expression and endogenous antigen presentation. *Int Immunol* 1998; **10**: 609–17.
22 Ito A, Matsuoka F, Honda H, Kobayashi T. Heat shock protein 70 gene therapy combined with hyperthermia using magnetic nanoparticles. *Cancer Gene Ther* 2003; **10**: 918–25.
23 Udono H, Srivastava PK. Comparison of tumor-specific immunogenicities of stress-induced proteins gp96, hsp90, and hsp70. *J Immunol* 1994; **152**: 5398–403.
24 Tamura Y, Peng P, Liu K, Daou M, Srivastava PK. Immunotherapy of tumors with autologous tumor-derived heat shock protein preparations. *Science* 1997; **278**: 117–20.
25 Moroi Y, Mayhew M, Trcka J *et al.* Induction of cellular immunity by immunization with novel hybrid peptides complexed to heat shock protein 70. *Proc Natl Acad Sci USA* 2000; **97**: 3485–90.
26 Kurotaki T, Tamura Y, Ueda G *et al.* Efficient Cross-Presentation by Heat Shock Protein 90-Peptide Complex-Loaded Dendritic Cells via an Endosomal Pathway. *J Immunol* 2007; **179**: 1803–13.
27 Kutomi G, Tamura Y, Okuya K *et al.* Targeting to static endosome is required for efficient cross-presentation of endoplasmic reticulum-resident oxygen-regulated protein 150-peptide complexes. *J Immunol* 2009; **183**: 5861–9.
28 Shen L, Sigal LJ, Boes M, Rock KL. Important role of cathepsin S in generating peptides for TAP-independent MHC class I crosspresentation in vivo. *Immunity* 2004; **21**: 155–65.

doi: 10.1111/j.1349-7006.2010.01623.x

Pigment Cell Melanoma Res. **24**; 63–74

PERSPECTIVE

Human hair melanins: what we have learned and have not learned from mouse coat color pigmentation

Shosuke Ito and Kazumasa Wakamatsu

Department of Chemistry, Fujita Health University School of Health Sciences, Toyoake, Aichi, Japan

CORRESPONDENCE Dr. Shosuke Ito, e-mail: sito@fujita-hu.ac.jp

KEYWORDS eumelanin/pheomelanin/hair melanin/cysteine/melanosome pH/mouse coat color

PUBLICATION DATA Received 28 June 2010, revised and accepted for publication 18 August 2010, published online 20 August 2010

doi: 10.1111/j.1755-148X.2010.00755.x

Summary

Hair pigmentation is one of the most conspicuous phenotypes in humans. Melanocytes produce two distinct types of melanin pigment: brown to black, indolic eumelanin and yellow to reddish brown, sulfur-containing pheomelanin. Biochemically, the precursor tyrosine and the key enzyme tyrosinase and the tyrosinase-related proteins are involved in eumelanogenesis, while only the additional presence of cysteine is necessary for pheomelanogenesis. Other important proteins involved in melanogenesis include P protein, MATP protein, α-MSH, agouti signaling protein (ASIP), MC1R (the receptor for MSH and ASIP), and SLC7A11, a cystine transporter. Many studies have examined the effects of loss-of-function mutations of those proteins on mouse coat color pigmentation. In contrast, much less is known regarding the effects of mutations of the corresponding proteins on human hair pigmentation except for MC1R polymorphisms that lead to pheomelanogenesis. This perspective will discuss what we have/have not learned from mouse coat color pigmentation, with special emphasis on the significant roles of pH and the level of cysteine in melanosomes in controlling melanogenesis. Based on these data, a hypothesis is proposed to explain the diversity of human hair pigmentation.

Introduction

Pigmentation of hair, skin, and eyes in animals is mainly a manifestation of the presence of melanin that is synthesized in melanocytes, within membrane-bound organelles termed melanosomes. Melanosomes in follicular or epidermal melanocytes are then transferred to surrounding keratinocytes to afford surprisingly diverse colors to hair and a wide range of color from light to dark in skin (Sturm, 2009). Melanocytes in mammals (and birds) produce two chemically distinct types of melanin, black to brown eumelanin and yellow to reddish brown pheomelanin (Ito, 2003; Ito and Wakamatsu, 2008). It is the quantity and the ratio of eumelanin to pheomelanin that mainly determines the color of hair, skin, and eyes (Ito and Wakamatsu, 2003).

Hair pigmentation is one of the most conspicuous phenotypes in humans. It is highly variable in color, ranging from black, dark brown, light brown, and blond to red. The underlying genetic basis for this diversity in human hair color has been a subject of extensive studies in recent years (Gerstenblith et al., 2010; McEvoy et al., 2006; Sturm, 2006, 2009). Those studies, especially genome-wide association studies (Han et al., 2008; Sulem et al., 2008), led to the identification of several genes involved in the normal variation of human hair color, including some previously unrecognized genes such as *TPCN2* (Sulem et al., 2008), *HERC2* (Han et al., 2008; Sturm et al., 2008), *IRF4* (Han et al., 2008), and *SLC24A4* (Han et al., 2008). In contrast, variations in mouse coat color have a long history of genetic as well as biochemical studies, as summarized in a classical treatise by Silvers (1979) and a review by Bennett and Lamoreux (2003). Increased interest in pigment research has resulted in the identification of a large number of new coat color genes. At present, 169

mouse coat color genes have been cloned, although 206 genes still remain to be cloned (http://www.espcr.org/micemut/). Among those 169 cloned mouse coat color genes, the majority are involved in the development of melanocytes and/or the construction and transport of melanosomes. However, fewer than 20 genes are directly involved in the production of melanin or in the regulation of the ratio of eumelanin to pheomelanin (Table 1). It should be stressed that congenic mice are available to study pigmentary effects of many specific coat color genes. Homologues of most of those genes are also involved in the variation of human pigmentation. Therefore, comparison of pigmentary effects of mouse coat color genes to those of human hair color genes should be informative. The effects of interactions between two (even three) coat color genes can be precisely analyzed in mice, but is not so straightforward in humans.

Biochemical/chemical background

Biochemical pathway for the production of eumelanin and pheomelanin

The biochemical pathway of melanogenesis has been described in detail in our recent reviews (Ito and Wakamatsu, 2008; Simon et al., 2009), and a brief summary of the scheme follows: both eumelanin and pheomelanin derive from the common precursor dopaquinone that is produced from tyrosine by the action of tyrosinase, the product of the *albino/Tyr* locus (Figure 1). Dopaquinone, an *ortho*-quinone, is a highly reactive intermediate, and in the absence of thiol compounds, it undergoes intramolecular cyclization to give cyclodopa (Land et al., 2003). Once formed, cyclodopa is rapidly oxidized to give dopachrome, a relatively stable intermediate. When not accelerated by any additional factors, dopachrome undergoes a mostly decarboxylative rearrangement to form 5,6-dihydroxyindole (DHI). However, a tyrosinase-related protein (Tyrp), called dopachrome tautomerase (Dct) or Tyrp2, the product of the *Dct/slaty* locus, catalyzes the tautomerization of dopachrome to 5,6-dihydroxyindole-2-carboxylic acid (DHICA) (Kroumpouzos et al., 1994; Pawelek et al., 1980; Tsukamoto et al., 1992). The dihydroxyindoles DHI and DHICA are then further oxidized to produce the eumelanin polymer. Oxidative polymerization of DHI is catalyzed directly by tyrosinase or indirectly by dopaquinone, while oxidation of DHICA appears to be catalyzed by Tyrp1, the *brown* locus protein, at least in mice (Jiménez-Cervantes et al., 1994; Olivares et al., 2001). However, the human homologue TYRP1 may not act in the same way as in mice (Boissy et al., 1998), and its precise enzymatic function in humans is not clear.

In contrast to eumelanogenesis, the production of pheomelanin appears to proceed spontaneously after the production of dopaquinone as long as cysteine is present (Ito and Wakamatsu, 2008; Land and Riley, 2000). Cysteinyldopa isomers are rapidly formed among which 5-*S*-cysteinyldopa is the major isomer (Ito and Prota, 1977). Oxidation of cysteinyldopas proceeds by redox exchange with dopaquinone to form the quinone form. Cyclization and rearrangement afford benzothiazine intermediates, which in turn gives rise to pheomelanin pigment (Wakamatsu et al., 2009). This whole

Table 1. Pigmentary functions of mouse color genes and the corresponding human genes involved in melanosome structure and function

Mouse symbol (synonym)	Gene name (locus)	Pigmentary function	Human symbol	Human disease or phenotype in loss-of-function mutation
(a) Components of melanosomes				
Tyr (c)	Tyrosinase (albino)	Melanogenesis	*TYR*	OCA1; dilution of skin/hair/eye color
Tyrp1 (b)	Tyrosinase-related protein 1(brown)	Eumelanogenesis	*TYRP1*	OCA3; dilution of skin/hair/eye color
Dct (slt)	Dopachrome tautomerase (slaty)	Eumelanogenesis	*DCT*	Not known
Oca2 (p)	Pink-eyed dilution	Tyrosinase trafficking; Neutralization of MS?	*OCA2/P*	OCA2; dilution of skin/hair/eye color
Slc24a5	Solute carrier family 24, member 5	Neutralization of MS	*SLC24A5/NCKX5*	Dilution of skin/hair/eye color
Slc45a2	Matp (underwhite)	Tyrosinase trafficking; Neutralization of MS?	*SLC45A2/MATP*	OCA4; dilution of skin/hair/eye color
Si	Silver	Melanosome genesis	*SILV/PMEL17*	Not known
(b) Eumelanin and pheomelanin switch				
A	Agouti	Switch to pheomelanogenesis	*ASIP*	Red hair (gain-of-function)
Atrn (mg)	Attractin (mahogany)	Switch to pheomelanogenesis	*ATRN*	Not known
Mc1r (e)	Melanocortin 1 receptor (extension)	Switch to eumelanogenesis	*MC1R*	Red hair
Pomc	Pro-opiomelanocortin	Switch to eumelanogenesis	*POMC*	Red hair
Slc7a11	Subtle gray (sut)	Cystine transport	*SLC7A11*	Not known

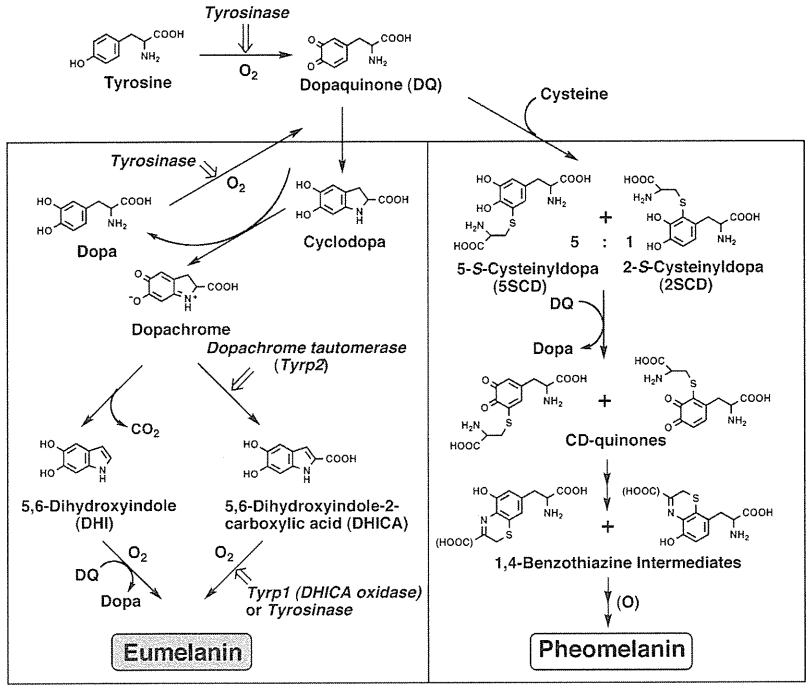

Figure 1. Biosynthetic pathways leading to eumelanin and pheomelanin production (adopted from Ito and Wakamatsu, 2008). Note that the activities of tyrosinase, Tyrp1 and Dct/Tyrp2 (and the precursor tyrosine) are involved in the production of eumelanin, while only tyrosinase (and the precursors tyrosine and cysteine) are necessary for the production of pheomelanin. (Figure used with permission, Blackwell Publishing.)

process of pheomelanogenesis requires only the activity of tyrosinase, in addition to the precursors, tyrosine and cysteine.

A three-step pathway for mixed melanogenesis

Melanogenesis in vivo produces mixtures (or copolymers) of eumelanin and pheomelanin. Therefore, melanogenesis should be considered as 'mixed melanogenesis'. We previously proposed a three-step pathway for mixed melanogenesis (Ito, 2003; Ito and Wakamatsu, 2008). In short, the total amount of melanin produced is proportional to dopaquinone production, which is in turn proportional to tyrosinase activity. Melanogenesis proceeds in three distinct stages: kinetic studies have shown that the initial stage is the production of cysteinyldopa isomers, which continues as long as the cysteine concentration is above 0.13 μM. The second stage is the oxidation of cysteinyldopas to produce pheomelanin, which is preferred over the production of eumelanin as long as cysteinyldopas are present at concentrations above 9 μM. The last stage is the production of eumelanin that begins only after most cysteinyldopas and cysteine are depleted. Therefore, the ratio of eumelanin to pheomelanin is determined by tyrosinase activity and the availability of tyrosine and cysteine in melanosomes, the branching point being 0.8 μM at pH 7.4 (Land and Riley, 2000; Land et al., 2003). More detailed discussion is presented by Ito and Wakamatsu (2008).

Chemical phenotype

Natural melanin pigments are mixtures (or copolymers) of eumelanin and pheomelanin. Although in most dark hairs of mammals, eumelanin is the predominant component, pheomelanin is a significant component in yellow/red hair in mice and in humans. Therefore, it is preferable to measure both eumelanin and pheomelanin so that the genotype can be correlated to the 'chemical phenotype' in a quantitative manner. Many studies use a melanin index measured with reflectometry as a quantitative marker of phenotype in the skin (e.g. Lamason et al., 2005; Stokowski et al., 2007) and in the hair (e.g. Mengel-From et al., 2009; Shekar et al., 2008a). Although this approach is quite useful to quantitatively evaluate pigmentation in large populations, such as the subjects in epidemiological studies, the method is somewhat limited because it is only an indirect measure of pigmentation.

We have previously established chemical methods to directly analyze eumelanin and pheomelanin contents based on the production of specific markers, pyrrole-2,3,5-tricarboxylic acid (PTCA) and aminohydroxyphenylalanine (AHP), respectively (Ito and Fujita, 1985; Wakamatsu and Ito, 2002). Our original methods used acidic permanganate oxidation and hydroiodic acid hydrolysis to produce PTCA and AHP isomers, respectively. That method was later improved so that AHP isomers are separated to 4-amino-3-hydroxyphenylalanine

(4-AHP) and its isomer 3-AHP, the former isomer being specific for 5-*S*-cysteinyldopa-derived pheomelanin so that the specificity for pheomelanin was increased (Wakamatsu et al., 2002). The acidic permanganate oxidation has now been replaced with alkaline hydrogen peroxide oxidation in which the yield of PTCA is doubled, and other markers can be simultaneously analyzed in a more simplified method (Wakamatsu et al., 2003). Notably, pyrrole-2,3-dicarboxylic acid (PDCA) can now be analyzed, and PTCA and PDCA can be used as markers to estimate DHICA- and DHI-derived units, respectively (Ito and Wakamatsu, 1998). As an independent parameter of pigmentation, we use absorbance at 500 nm after solubilization in aqueous Soluene-350 (Ozeki et al., 1995, 1996).

We have used these chemical degradation methods to evaluate the diversity of human hair pigmentation. Chemical phenotypes were analyzed for 209 University of Arizona students (our unpublished results). Except for red hair, human hair melanins consist of approximately 99% eumelanin. Dark brown hair (n = 53) contains eumelanin at 64% the level of black hair (n = 82), medium to light brown hair (n = 43) at 46%, and blond brown to blond hair (n = 23) at 23%. On the other hand, red hair (n = 8) contains eumelanin at 31% the level of black hair and pheomelanin at a level comparable to eumelanin. Similar results with red hair have been reported in Naysmith et al. (2004). So, how is this diversity in human hair pigmentation biochemically controlled? This is the major question addressed in this Perspective.

Effects of mutations on mouse/human pigmentation

Tyr/ *TYR* locus

The enzyme tyrosinase is encoded at the *albino*/*Tyrosinase* (*C*) locus in mice. Tyrosinase is the key enzyme in melanogenesis, producing dopaquinone that is a common precursor for eumelanin and pheomelanin (Figure 1). Without functional tyrosinase, no melanin is produced in mice or in humans (in humans, this is termed oculocutaneous albinism type 1, OCA1) (Oetting and King, 1999; Suzuki and Tomita, 2008). The *chinchilla* allele at the *albino* locus encodes a partially functional tyrosinase whose activity is <50% wild type, because of a point mutation (Ala464Thr) that makes it susceptible to proteolytic cleavage (Müller et al., 1988). Thus, this mutant is an ideal model to examine the specific effects of tyrosinase activity on melanogenesis. Mice homozygous for the *chinchilla* allele have eumelanin contents about 50% that contained in *nonagouti* black hairs (Lamoreux et al., 2001). However, this suppression was not observed in *chinchilla* mice homozygous also for *slaty* (Dct^{slt}/Dct^{slt}) or *brown* ($Tyrp1^{b}/Tyrp1^{b}$) to significant extents (Table 1). Interestingly, homozygosity for the *chinchilla* allele greatly reduces the amount of pheomelanin both in *lethal yellow* (A^{y}/a) and in *recessive yellow* ($Mc1r^{e}/Mc1r^{e}$) mice by >80%.

These results with *chinchilla* mice indicate that functional Dct and Tyrp1 are also necessary, in addition to high levels of tyrosinase, for maximal production of eumelanin. On the other hand, the greatly reduced production of pheomelanin in *chinchilla* mice with *lethal yellow* or *recessive yellow* mutation can be explained by the three-step theory of melanogenesis noted earlier. It is likely that under conditions of low tyrosinase activity (and high cysteine concentration), cysteinyldopas are produced, but are not readily oxidized to pheomelanin (Ito and Prota, 1977; Ito and Wakamatsu, 2008). In *black* (*nonagouti*) *chinchilla* mice, the degree of eumelanogenesis can be directly proportional to tyrosinase activity under low cysteine concentration.

Mutations at the *TYR* locus in humans cause OCA1 with various degrees of pigmentation. SNPs in *TYR* genes are also known to affect normal pigmentation in humans (Sturm, 2009). However, those mutations do not seem to play major roles leading to the diversity of human hair pigmentation (Sturm, 2009; Valenzuela et al., 2010). It would be interesting to know whether human red hair caused by a mutation in *MC1R* would be affected by a mutation in tyrosinase that decreased its activity, a situation similar to *recessive yellow chinchilla* mice.

Dct/*DCT* and *Tyrp1*/*TYRP1* loci

The *slaty*/*Dct* (*Slt*) locus in mice encodes Tyrp2/Dct that catalyzes the tautomerization of dopachrome to DHICA, and thus wild-type mice produce DHICA-rich eumelanin. This is indicated by high values of PTCA/total melanin ratios in mice wild-type at the *slaty* locus, including *black*, *brown*, *black chinchilla*, and *brown chinchilla* mice (Lamoreux et al., 2001). Homozygosity for the mutant *slaty* allele results in Dct whose functional activity is reduced 3- to 10-fold (Jackson et al., 1992) or null (our unpublished observation). This mutant *slaty* genotype was found to greatly reduce the PTCA value with a mild reduction in total melanin, and hence, the PTCA/total melanin ratio was reduced four to sixfold, indicating the production of DHICA-poor eumelanin.

Polymorphisms in the *DCT* gene in humans are known and are believed to affect hair pigmentation, at least in Asians (McEvoy et al., 2006). However, it is not known whether such polymorphisms play a major role in producing the lighter color in the skin (and hair) of Asians compared to Africans. Interestingly, follicular melanocytes of brown or black hairs were found to lack expression of DCT protein irrespective of ethnic origin (Commo et al., 2004). This would result in the production of DHICA-poor eumelanin in human hair. However, systematic studies evaluating the ratio of DHI to DHICA in human hair remain to be carried out.

Tyrp1 is encoded at the *brown*/*Typr1* (*B*) locus and is believed to act as a DHICA oxidase in mice

(Jiménez-Cervantes et al., 1994; Kobayashi et al., 1994b). The *brown* mutation encodes Tyrp1 that is not properly translocated to melanosomes, resulting in no functional Tyrp1 activity and decreased tyrosinase function. Homozygosity for the mutant *brown* allele significantly suppresses the production of eumelanin (total melanin and PTCA values), as evidenced by comparing wild-type *black* with *brown* and of *black chinchilla* with *brown chinchilla*. The *brown* mutation does not significantly alter the proportion of DHICA in the eumelanin synthesized, but rather, *brown* eumelanin appears to have a smaller molecular size compared to wild-type *black* eumelanin (Ozeki et al., 1997).

In humans, TYRP1 does not appear to function as a DHICA oxidase (Boissy et al., 1998). Although the exact enzymatic function of TYRP1 is not known, it appears to stabilize tyrosinase (and DCT) in mice and in humans (Kobayashi et al., 1998). It is not known whether polymorphisms in the *TYRP1* gene affect normal human pigmentation. However, one mutation at this gene, called OCA3, has been reported to alter the black hair color in Africans to brown (Boissy et al., 1996). A similar hypopigmentation effect caused by OCA3 was also observed in one Caucasian (Rooryck et al., 2006).

Oca2 (p)/OCA2 (P), Slc24a5/SLC24A5 (NCKX5), Slc45a2/SLC45A2 (MATP), and *Si/SILV (PMEL17)* loci

The *pink-eyed dilution* (*p*) gene (now called *Oca2* gene) in mice encodes an integral melanosomal membrane protein with a 12-membrane-spanning structure, and mutations at this locus suppress eumelanin production (Rosemblat et al., 1994), reducing it more than 10-fold (Ozeki et al., 1995). Interestingly, *p*-mutant melanocytes secrete most of the melanin they produce to the culture medium (Hirobe et al., 2002). A similar observation was reported with melan-p1 melanocytes by Potterf et al. (1998). Also, *pink-eyed dilution* mice secrete high levels of melanin-related metabolites, such as 5-*S*-cysteinyldopa, into the blood compared to wild-type mice (Wakamatsu et al., 2007). Thus, it seems likely that the *p* mutation causes a defect in retaining melanin and melanin precursors in melanosomes. Alternatively, the *p* mutation disrupts tyrosinase processing and intracellular trafficking to melanosomes, thus suppressing their normal maturation (Ni-Komatsu and Orlow, 2006; Toyofuku et al., 2002).

Mutations at the *OCA2* (*P*) locus in humans cause reductions in eumelanin production and null mutations lead to another form of oculocutaneous albinism, OCA2 (Suzuki and Tomita, 2008). Several SNPs of the *OCA2* gene are associated with hair or skin color variations in Australians and in East Asians (Edwards et al., 2010; Shekar et al., 2008b). A single SNP in the *HERC2* gene, which functions upstream of *OCA2* has been postulated to lead to decreased expression of OCA2 protein within melanocytes. It is a causative SNP for blue eye color with effects also apparent on skin and hair color (Branicki et al., 2009; Cook et al., 2009; Sturm, 2009).

Mutations in the *Slc24a5* gene have not been found in mice, probably because the mutant is indistinguishable from wild-type mice (Vogel et al., 2008). Instead, the mutation was originally found in *golden* zebrafish and in humans (Lamason et al., 2005). The *Slc24a5* gene encodes a potassium-dependent sodium–calcium exchanger denoted NCKX5 (Ginger et al., 2008). The evolutionarily conserved ancestral allele of a human coding polymorphism, Ala111Thr, predominates in African and in East Asian populations, while the variant allele is nearly fixed in European populations (Sturm, 2009). That polymorphism correlates with lighter skin pigmentation in admixed populations, accounting for 25–38% of the difference in skin color between Europeans and Africans (Lamason et al., 2005).

The *Slc45a2* (*underwhite*) locus in mice encodes a membrane-associated transporter protein (Matp) that has a 12-transmembrane-spanning structure (Newton et al., 2001). The mutations (*uw*, uw^{d}, and UW^{dbr}) at the *underwhite* locus reduce the production of eumelanin >90% compared to wild-type mice (Lehman et al., 2000). The hypopigmentary effect of the *underwhite* mutation is independent of *p*, because double mutant mice at *uw* and *p* have an *albino* appearance. The pigmentary function of Matp is not fully clarified. However, Costin et al. (2003) reported that processing and trafficking of tyrosinase to melanosomes is disrupted and tyrosinase is abnormally secreted from *underwhite* mouse melanocytes, a process similar to that seen in *p* melanocytes.

The orthologue of *underwhite* in mice was identified in medaka as the *b/Aim1* gene (Du and Fisher, 2002; Fukamachi et al., 2001) and then in humans as the *MATP* gene, mutations of which cause severe hypopigmentation, named OCA4 (Inagaki et al., 2004; Newton et al., 2001). The ancestral allele of the *MATP* coding polymorphism is also known; the 374Leu allele predominates in Africans and in East Asians, while the 374Phe allele is found at high frequency in Europeans (Sturm, 2009). The 374Leu polymorphism is highly associated with black hair (Branicki et al., 2008; Graf et al., 2005).

Pigmentary effects of mutations in the *OCA2* (*P*), *SLC45A2* (*MATP* or *OCA4*), and *SLC24A5* (*NCKX5*) genes in humans have been studied extensively in recent years. Most of those studies were aimed at identifying polymorphisms that cause the diversity in normal pigmentation in the skin, hair, and eyes between and within human populations (McEvoy et al., 2006; Stokowski et al., 2007; Sturm, 2006, 2009). However, biochemical studies that correlate those genotypes to chemical phenotypes are limited (Cook et al., 2009; Valenzuela et al., 2010).

Mutations at the *silver* (*Pmel17*) locus affect eumelanin production only slightly (20% reduction) on *nonagouti* background. However, the effects become more pronounced (40–50% reduction) when interacting with the *brown* locus (Lamoreux et al., 2001). Thus, the effects of mutations at the *brown* and *silver* loci are additive. The silver protein is important to the biogenesis of early stage melanosomes (Kobayashi et al., 1994a; Theos et al., 2005) and is required for and is the primary component of the matrix fibrils in eumelanosomes (Theos et al., 2006). In humans, the homologue *SILV* (*PMEL17*) has not been linked with hair pigmentation.

A/ASIP, Atrn/ATRN, Mc1r/MC1R, Pomc/POMC, and *Slc7a11/SLC7A11* loci

The pigment type switching between eumelanogenesis (black in mice and black to dark brown in humans) and pheomelanogenesis (yellow in mice and red in humans) has been studied extensively in the past 15 yr since human MC1R polymorphisms that cause the red hair color (RHC) phenotype were discovered (Rees, 2003; Valverde et al., 1995).

The master regulator of pigment-type switching is the melanocortin-1 receptor (Mc1r/MC1R). Briefly, when α-MSH binds MC1R on the plasma membrane of melanocytes, adenyl cyclase is activated through the stimulatory G-protein, raising levels of the second messenger cAMP, thereby activating the melanogenic transcription factor MITF (Bertolotto et al., 1998; Walker and Gunn, 2010). This leads to upregulation of many genes required for pigment production such as *TYR, TYRP1, DCT, OCA, SLC24A5*, and many others (Le Pape et al., 2009; Levy et al., 2006; Spry et al., 2009). Agouti signaling protein (Asip/ASIP), encoded by the *A/ASIP* gene, is a competitive antagonist that inhibits the eumelanogenic effect of α-MSH by competing with it for binding to the MC1R. Using cDNA microarrays, Le Pape et al. (2009) demonstrated that ASIP blocks the transcriptional effects of α-MSH.

Burchill et al. (1986) examined the effects of α-MSH on mixed melanogenesis in *viable yellow* mice. When pubertal mice producing a mixed-type melanin were injected with α-MSH, tyrosinase activity increased twofold and more eumelanic hair was produced with a concomitant increase in total melanin. When those pubertal mice were injected with bromocriptine (which reduces α-MSH secretion), tyrosinase activity was greatly reduced and pheomelanic hair was produced along with a decrease in total melanin. These results clearly indicate a significant role of tyrosinase activity in controlling mixed melanogenesis; higher tyrosinase activities favor eumelanogenesis, while lower activities favor pheomelanogenesis.

Asip requires two accessory proteins for pigment-type switching; the products of the *mahogany (mg)* and *mahoganoid (md)* loci (Walker and Gunn, 2010). The *mahogany* locus was identified as the mouse orthologue of the human *attractin (ATRN)* gene, and the *mahoganoid* locus encodes a novel RING-domain-containing protein. Mice homozygous for *mahogany* and heterozygous for *lethal yellow* produce a mixed-type melanin with a low level of eumelanin (<15% of *nonagouti black*) and have a reduced level of pheomelanin (~60% of *lethal yellow*). Similarly, Gunn et al. (2001) found that three *Atrn* mutants, either homozygous or compound heterozygous, showed a pheomelanin content 5- to 10-fold lower than wild-type agouti C3H/HeJ mice. The chemical phenotype of *mahoganoid* mice has not been studied. In humans, pigmentary effects of mutations in the human orthologues, ATRN and MGRN1, are not known.

Another control point in mixed melanogenesis is the concentration of cysteine in melanosomes (del Marmol et al., 1996). Chintala et al. (2005) demonstrated that the subtle gray (*sut*) mutation in mice arose because of a mutation in the *Slc7a11* gene that encodes the plasma membrane cystine/glutamate exchanger xCT. The resulting low rate of extracellular cystine transport into *sut* melanocytes reduces pheomelanin production with minimal or no effect on eumelanin production. In fact, the effect of the *sut* mutation on pheomelanin production was markedly accentuated on the A^y/a background, reducing pheomelanin levels in hair to one-sixth of the control level. In humans, no mutations in SLC7A11 are known to affect pigmentation.

In humans, several polymorphisms of the *MC1R* gene cause the RHC phenotype (Rees, 2003; Valverde et al., 1995). We have shown that RHC polymorphisms in *MC1R* can account for 67% variance of log values of eumelanin to pheomelanin ratio (Naysmith et al., 2004). Polymorphisms in other genes such as *OCA2, SLC45A2,* and *SLC24A5* may also contribute to the RHC phenotype in an additive manner (King et al., 2003; Valenzuela et al., 2010). A polymorphism in *ASIP* gene shows strong association with red hair (Sulem et al., 2008).

Mutations in the *proopiomelanocortin* (*POMC*) gene, which encodes the propeptide for α-MSH, cause red hair in humans, although only in rare cases (Krude et al., 1998). Interestingly, we found a case of a POMC mutation in a patient of African ancestry who did not exhibit the RHC phenotype or hypopigmentation (Clément et al., 2008). It was suggested that MC1R in this patient has a constitutive activity exhibited in the absence of its ligand α-MSH. The constitutive activity of Mc1r has been observed in mice; hairs of *nonagouti* mice lacking *Pomc* are indistinguishable from those of $Pomc^+$ mice (Slominski et al., 2005), although on *agouti* background (in the presence of agouti signaling protein) *Pomc*-null mice are more yellowish than $Pomc^+$ mice (Walker and Gunn, 2010; Yaswen et al., 1999).

What we have learned and have not learned from mouse coat color pigmentation

More than 300 pigmentary genes are known in mice. Mutations in those coat color genes have provided mice

with a diverse spectrum of colors, ranging from black, brown, light brown, gray, to yellow (Silvers, 1979). As have been discussed earlier, most of pigmentary genes in humans find the corresponding orthologues in mice that have been identified prior to the human orthologues. Thus, the progress in pigmentation research in the past 30 yr enjoyed the benefits from using those mutant mice or melanocytes isolated from them. However, the rapid upsurge in genetic studies has found pigmentary genes in humans that do not have precedents in mice. Typical examples are *SLC24A5* (Lamason et al., 2005) and *TPCN2* (Calcraft et al., 2009). The lack of mouse models of those mutants appears to stem from the fact that mutations in those genes would not have caused dramatic changes in mouse coat color. Another problem in relying on mouse models seems that coat color mutations in mice often lead to a complete loss-of-function with a drastic reduction in melanin content or a distinct change in eumelanin to pheomelanin ratio. On the contrary, diversity in normal human pigmentation is likely to result from the interaction of multiple genes with only a partial loss-of-function (Branicki et al., 2009; Cook et al., 2009; Sturm, 2009; Valenzuela et al., 2010). However, studies with double mutant or even triple to quadruple mutant mice would give valuable information regarding interaction of the coat color genes involved (Chintala et al., 2005; Gautam et al., 2006; Lamoreux et al., 2001; Lehman et al., 2000). Also, a caution should be given to the fact that proteins encoded by the same genes in mice and humans do not necessarily function in the same way; an example is found in Tyrp1/TYRP1 (Boissy et al., 1998).

Perspective for the diversity in human hair pigmentation

Effects of acidic pH on mixed melanogenesis

The role of pH in controlling mixed melanogenesis is now receiving much attention because it was recently found that melanosomes in melanocytes from White/fair skin are acidic, while those from Black/dark skin are near neutral (Smith et al., 2004). Also, tyrosinases from White and Black melanocytes have the same optimum at pH 7.4 with greatly reduced activities at acidic pHs; activities at pH 5.8 were ~20% those at pH 6.8 (Fuller et al., 2001). Furthermore, the great diversity in normal human skin pigmentation appears to stem from polymorphisms in only several genes, including *OCA2*, *MATP*, and *SLC24A5* (Lamason et al., 2005; Lao et al., 2007; Norton et al., 2007). Available evidence suggests that polymorphisms in those genes may result in the acidification of melanosomes. However, the significance of pH in controlling mixed melanogenesis has only been addressed directly in a study by Ancans et al. (2001). They showed by neutralizing intramelanosomal pH in cultured human melanocytes and in melanoma cells that cells with greatly increased tyrosinase activity after neutralization had a preferential increase in the production of eumelanin with an increase in the eumelanin to pheomelanin ratio. A recent study has shown that activation of the cAMP pathway by α-MSH or forskolin leads to an alkalization (neutralization) of melanosomes and a fourfold increase in melanin content (Cheli et al., 2009). Although that study links the pH of melanosomes to the cAMP pathway for the first time, the issue of mixed melanogenesis was not examined.

A hypothetical model for roles of transporters for melanin precursors and ions

Human hair pigmentation is very diverse, especially among Europeans. The genetic basis for the RHC phenotype has been largely attributed to mutations in *MC1R*. Biochemically, as shown in Figure 1, the presence of a minimal level of cysteine is essential for pheomelanogenesis as seen in red hair. However, much less is known about the genetic and biochemical basis for the blond phenotype. The chemical phenotype of blond brown to blond hair indicates that those light-colored hairs are essentially eumelanic, similar to black, but with only 25% the eumelanin content. Thus, the blond phenotype requires not only low levels of tyrosinase activity but also low (to trace) levels of cysteine to avoid the production of pheomelanin. This could be achieved through the acidification of melanosomes and the efflux of cysteine (or cystine) from them.

Tyrosinase is transferred to stage II melanosomes together with Tyrp1 and Tyrp2/DCT (Costin et al., 2003) and is involved in the production of pheomelanin and eumelanin. Melanogenesis also requires the melanin precursors, tyrosine and cysteine, which are actively taken up into melanosomes through specific transport systems (Potterf et al., 1996, 1999; Figure 2).

An acidic pH should be considered to explain the lower levels of pigmentation produced in Europeans. Lamason et al. (2005) proposed that SLC24A5 is involved in hypopigmentary effects through its activity as the potassium-dependent sodium–calcium exchanger NCKX5. Neutralization of melanosomal pH can be achieved through a cascade of ion transporters as shown in Figure 2. Thus, several vacuolar proton ATPases are known to be located in melanosomes (Tabata et al., 2008). Protons taken up are then effluxed through sodium–proton exchangers. Actually, several sodium–proton exchangers are present both in Black and in White melanocytes, and some are found in melanosomes (Smith et al., 2004). It would be interesting to determine whether SLC45A2 (MATP) and/or OCA2 (P) proteins act as sodium–proton exchanger(s) (Sturm, 2006), because those melanosomal proteins are believed to be transporters with 12-membrane-spanning structures. Sodium ions taken up by the sodium–proton exchangers are then effluxed through SLC24A5 (NCKX5). It should be noted that SLC45A2 and SLC24A5 are actually present in melanosomes, as

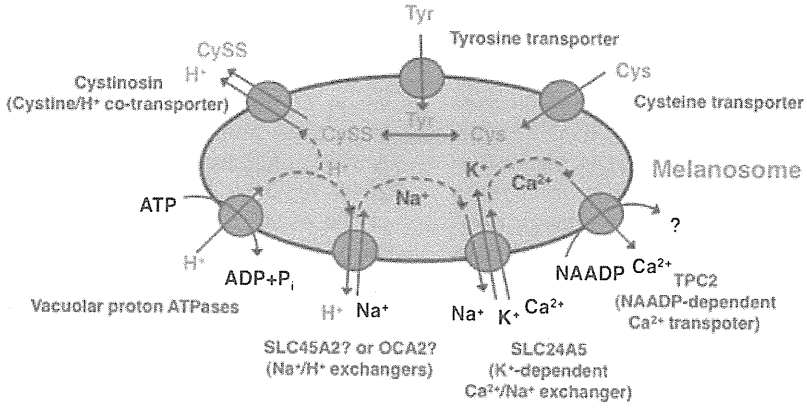

Figure 2. Roles of transporters for melanin precursors and various ions. Tyrosine (Tyr) and cysteine (Cys), precursors of eu- and pheomelanin, are actively transported into melanosomes. Cysteine and its oxidized dimer cystine (CySS) are convertible through redox exchange. Cystine is pumped out by cystinosin (CTNS), a cystine/H^+ cotransporter. Proton levels (acidity) of melanosomes are regulated through a cascade of four different ion transporters, vacuolar proton ATPases (H^+ influx), Na^+/H^+ exchangers (H^+ efflux and Na^+ influx), SLC24A5 (Na^+ efflux and Ca^{2+}, K^+ influx), and TPC2 (Ca^{2+} efflux). The net results of maximal activity of those transporters would be a low acidity (neutral pH), a high tyrosine level, a low cysteine level (and a high K^+ level), leading to proeumelanogenic conditions (dark hair phenotype). Polymorphisms of ion transporters would make melanosomes acidic, leading to the suppression of eumelanogenesis (light hair phenotype). Polymorphisms of MC1R would result in the downregulation of tyrosinase as well as these transporters, leading to a switch to pheomelanogenesis (red hair phenotype). For more details, see the Text.

proved by a proteomics study (Chi et al., 2006). Thus, acidification of melanosomes would result from several polymorphisms in the *SLC45A2* (and *OCA2*) and *SLC24A5* genes. It should be added that tyrosinase is properly trafficked to melanosomes only when intracellular organelles are neutralized (Watabe et al., 2004).

The above-mentioned hypothetical model requires calcium (and potassium) ions to be accumulated in melanosomes. In this regard, it should be noted that a newly identified TPC2 (two-pore segment channel 2), the product of the *TPCN2* gene, mediates nicotinic acid adenine dinucleotide phosphate (NAADP)-dependent calcium ion transport from lysosome-related acidic compartments (Calcraft et al., 2009). It is possible that TPC2 acts in concert with SLC24A5 to lower calcium levels in melanosomes (Figure 2). In this regard, it should be added that two polymorphisms of *TPCN2* are associated with blond hair color compared to brown hair color (Sulem et al., 2008).

Once the acidification of melanosomes is achieved, the levels of cysteine (or cystine) need to be regulated. We propose that this could be achieved through the activity of cystinosin/CTNS, a cotransporter of cystine/proton in lysosome-related organelles (Kalatzis et al., 2001). Cystinosis is an inherited lysosomal storage disease characterized by the defective transport of cystine, because of mutations of the *cystinosin/CTNS* gene (Town et al., 1998). The efflux of cystine from lysosomes by cystinosin is coupled to an efflux of protons. It has been shown that CTNS is localized in melanosomes and controls their pH (Ortonne, 2010; C. Chiaverini, R. Ballotti, and J.P. Ortonne, in submission). The chemical phenotypes of 27 cystinosis patients have now been analyzed. In patients, eumelanin levels are reduced 50%, while pheomelanin levels are increased twofold compared with normal family members. Together, the eumelanin to pheomelanin ratio is reduced fivefold (our unpublished results). Thus, the acidification of melanosomes together with cystine accumulation in cystinosis patients causes hypopigmentation with a partial shift to pheomelanogenesis. Conversely, it appears likely that cystine levels (hence cysteine levels through redox exchange with GSH) in melanosomes would be low as long as cystinosin functions properly. It should be added that a high potassium concentration, which can be achieved through the cascade of ion transporters (Figure 2), is favorable for the maximal efflux of cystine (and protons) (Smith et al., 1987).

In light of these considerations of melanosomal pH and cysteine levels, we propose a hypothesis for the control of human hair pigmentation based on the activities of melanosomal transporters (Table 2). The 'dark' hair phenotype, black to dark brown hair, is characterized by high levels of MC1R signaling and full activities of ion transporters and cystinosin, the cystine transporter. Under these promelanogenic conditions, melanosomes become neutral and cysteine deficient, leading to the production of high levels of eumelanin.

The 'light' hair phenotype, light brown to blond hair, is characterized by high levels of MC1R signaling, reduced activities of ion transporters because of polymorphisms, and full activity of cystinosin. Under these suppressed, but proeumelanogenic conditions, melanosomes become acidic and cysteine deficient, leading to the production of lower levels of eumelanin. One may be

Table 2. Biochemical characteristics of three major phenotypes of human hair pigmentation

Characteristic	Dark hair	Light hair	Red hair
Color of hair	Black to dark brown	Light brown to blond	Red
MC1R	Functional	Functional	Not functional
SLC24A5/SLC45A2?/OCA2?/TPC2	Functional	Not functional	Functional (low)
CTNS	Functional	Functional	Functional (low)
Melanosomal pH	Near neutral	Acidic	Acidic
Melanosomal Cys (CySS)	Low	Low	High
Melanin	High eumelanin	Low eumelanin	Low pheomelanin (+ low eumelanin)

Note: Neutral pH in the strict sense is pH 7.0 and 6.8 at 25°C and 37°C, respectively, as the dissociation constant of water is 10^{-14} at 25°C and $10^{-13.6}$ at 37°C.

surprised to know that blond hair contain mostly eumelanin, considering the rather yellowish tint of its hair color. It would be possible that eumelanin polymers produced under these 'suppressed' conditions may be smaller in molecular size thus providing lighter, yellowish color to 'blond' hair.

Lastly, the 'red' hair phenotype is characterized by low levels of MC1R signaling, leading to the downregulation of various genes through *MITF*, the master gene that controls melanogenesis (Walker and Gunn, 2010). Those genes include *TYR, TYRP1, DCT, OCA2, SLC24A5,* and *SLC45A2* (Le Pape et al., 2009). The *CTNS* gene should also be downregulated, leaving high levels of cystine (hence cysteine) inside melanosomes. Under these suppressed, but propheomelanic conditions, melanosomes become acidic but cysteine rich, leading to the production of low levels of pheomelanin (and eumelanin).

Future directions to a better understanding of human hair pigmentation

One important unsolved problem in melanogenesis is the precise mechanism of switching between eumelanogenesis and pheomelanogenesis in vivo (Walker and Gunn, 2010). Biochemically, that switching appears to depend on tyrosinase activity as well as on the availability of cysteine (or cystine) in melanosomes. In this connection, the role of the cystine transporter Slc7a11 (Chintala et al., 2005) in regulating mixed melanogenesis deserves more attention. It would be interesting to determine whether SLC7A11 (or another transporter) acts as a transporter taking cystine into melanosomes. Also, a recent study suggests the presence of additional factor(s) controlling pheomelanogenesis (Hida et al., 2009). Certainly, further studies are needed to understand how cysteine (and cystine) levels in melanosomes are regulated.

The roles of transporters in regulating melanosomal pH and cysteine level, as proposed in Figure 2 and Table 2, requires several confirmations. SLC45A2 and/or OCA2 proteins need to be shown to act as sodium–proton exchangers. Biochemical studies on the TPC2 protein will be required to confirm the calcium ion transporter activity in melanosomes. The roles of calcium ions in melanosomes also need to be studied. Finally, the involvement of cystinosin as a cotransporter for cystine/proton in melanosomes awaits clarification. Another interesting problem that needs to be clarified is how the yellowish color of eumelanin in blond hair can be produced in acidic environments.

In addition to the suppression of tyrosinase activity, pheomelanogenesis is kinetically favored under a more acidic environment because the cyclization of dopaquinone (the first step in eumelanogenesis) proceeds much slower at lower pHs, while the cysteinyldopa quinone cyclization (yielding the first bicyclic intermediate in pheomelanogenesis) proceeds faster (Thompson et al., 1985). Future studies will no doubt further elucidate the biochemical control of mixed melanogenesis in an acidic environment.

Acknowledgements

The authors acknowledge valuable comments by Dr. Vincent J. Hearing, NIH, USA. They also thank Prof. Jean-Paul Ortonne, University of Nice, Sophia Antipolis, France for the permission to cite their unpublished data. This work was supported, in part, by a Japan Society for the Promotion of Science (JSPS) grant (No. 20591357).

References

Ancans, J., Tobin, D.J., Hoogduijn, M.J., Smit, N.P., Wakamatsu, K., and Thody, A.J. (2001). Melanosomal pH controls rate of melanogenesis, eumelanin/phaeomelanin ratio and melanosome maturation in melanocytes and melanoma cells. Exp. Cell Res. *268*, 26–35.

Bennett, D.C., and Lamoreux, M.L. (2003). The color loci of mice – a genetic century. Pigment Cell Res. *16*, 333–344.

Bertolotto, C., Abbe, P., Hemesath, T.J., Bille, K., Fisher, D.E., Ortonne, J.P., and Ballotti, R. (1998). Microphthalmia gene product as a signal transducer in cAMP-induced differentiation of melanocytes. J. Cell Biol. *142*, 827–835.

Boissy, R.E., Zhao, H., Oetting, W.S. et al. (1996). Mutation in and lack of expression of tyrosinase-related protein-1 (TRP-1) in mela-